https://doi.org/10.5194/bg-2022-164
Preprint. Discussion started: 18 August 2022

Biogeosciences Discussions

Assessing carbon storage capacity and saturation across six central US grasslands using data-model integration

Kevin R. Wilcox[1], Scott L. Collins[2], Alan K. Knapp[3], William Pockman[2], Zheng Shi[4], Melinda D. Smith[3], Yiqi Luo[5]

[1]Department of Ecosystem Science and Management, University of Wyoming, Laramie, WY 82071, USA
[2]Department of Biology, University of New Mexico, Albuquerque, NM, 87131, USA
[3]Department of Biology & Graduate Degree Program in Ecology, Colorado State University, Fort Collins, CO, 80523, USA
[4]Department of Microbiology and Plant Biology, University of Oklahoma, Norman, OK, 73019
[5]Department of Biological Sciences, Center for Ecosystem Science and Society, Northern Arizona University, Flagstaff, AZ, 86011, USA

Correspondence to: Kevin R. Wilcox (kevin.wilcox@uwyo.edu)

Abstract. Future global changes will impact carbon (C) fluxes and pools in most terrestrial ecosystems and the feedback of terrestrial carbon cycling to atmospheric CO_2. Determining the vulnerability of ecosystems to future changes in C is thus vital for targeted land management and policy. The C capacity of an ecosystem (X_C) is a function of its C inputs (*e.g.*, net primary productivity – NPP) and how long C remains in the system before being respired back to the atmosphere (ecosystem C residence time – τ_E). The proportion of X_C currently stored by an ecosystem (*i.e.*, its C saturation – C_{SAT}) provides information about the potential for long-term C pools to be altered by environmental and land management regimes. We estimated X_C, C_{SAT}, NPP, and τ_E in six US grasslands spanning temperature and precipitation gradients by integrating high temporal resolution C pool and flux data with a process-based C model. As expected, NPP across grasslands was strongly correlated with mean annual precipitation (MAP), while τ_E was primarily a function of mean annual temperature (MAT). We link soil temperature, soil moisture, and inherent C turnover rates (potentially due to differences in microbial function) as determinants of τ_E. Overall, we found that intermediates between extremes in moisture and temperature had low CSAT, indicating that ecosystem C in these systems may be buffered against global change impacts on X_C. Hot and dry grasslands had greatest C_{SAT} due to both small C inputs through NPP and high C turnover rates during periods of favorable soil conditions. C_{SAT} also was high in tallgrass prairie due to frequent fire that reduced inputs of aboveground plant material. Accordingly, we suggest that both hot, dry ecosystems and those frequently disturbed should be subject to careful land management and policy decisions to prevent losses of C stored in these systems.

1 Introduction

In the coming decades, most terrestrial ecosystems will experience changes in environmental drivers, including increased air temperatures and atmospheric CO_2 concentrations, altered precipitation amounts and patterns, changes in fire frequency, and

https://doi.org/10.5194/bg-2022-164
Preprint. Discussion started: 18 August 2022

various anthropogenic impacts (e.g., agriculture)(IPCC, 2022). These changes are likely to have strong impacts on ecosystem functioning, such as C assimilation via plant growth or C losses via respiration (Hungate et al., 1997, Wang et al., 2016, Naylor et al., 2020). These will in turn affect critical ecosystem services, such as C sequestration (Lal, 2004, Wiesmeier et al., 2019). Information about which ecosystems may experience the greatest changes in C storage when subjected to future environmental change is important for targeted land management (Rees et al., 2005) and policy decisions (Daily et al., 2009). Experimental studies offer a way to assess how global changes are likely to impact ecosystem processes. Yet, experiments often have difficulty tracking effects on C storage since changes in soil C pools can take decades (Balesdent el al., 1988; Chapin et al., 2011), and most experiments are conducted for relatively short time periods. Process-based models offer another method to assess alterations in soil C under future conditions. Yet, variation of ecosystem properties and processes controlling C cycling across ecosystems, such as microbial community composition, is not well represented in many current models. Additionally, uncertainty surrounding ecosystem C is currently very large (Todd-Brown et al., 2014, Friend et al., 2014, Luo et al., 2015, Sulman et al., 2018). This highlights the need for better understanding of how C processes (and thus model parameters) vary across ecosystems.

Luo et al. (2017) introduced carbon capacity (X_C) as the amount of C that would be stored in soil and vegetation in an ecosystem if given enough time to reach equilibrium under current environmental conditions. Comparisons of X_C and the amount of C currently stored by that system allows for identification of ecosystems that are vulnerable to C loss under global change. In most terrestrial ecosystems, X_C is primarily a function of C inputs (NPP) and the amount of time that carbon remains in a system before being respired back to the atmosphere (ecosystem C residence time - τ_E, Luo et al., 2017). There are often mismatches between the amount of C currently stored within ecosystems and a system's X_C because C recovery from previous disturbances/environmental conditions can take decades or centuries (e.g., tillage, Smith, 2014). This may underlie observations of grasslands acting as strong C sinks (Soussana et al., 2007). The long-term trajectory (e.g., gains or losses) of C in an ecosystem can be inferred through a comparison of its C storage at present (X_P) with its X_C (Fig. 1a). It follows that global changes that affect X_C – through impacts on NPP and/or τ_E – are likely to have significant impacts on long-term C trajectories if X_P is close to X_C (Fig. 1b). Alternately, C trajectories where X_P is far below X_C may be less vulnerable to global change scenarios as long as X_P remains below future X_C (Fig. 1c). Therefore, we suggest that the proportion of X_C that is currently present in ecosystems (hereafter termed C saturation – C_{SAT}) may be used as an indicator of how vulnerable C pools are to future changes in environmental drivers.

Geographic patterns of X_C depend on how its components (NPP and τ_E) vary across ecosystems and environmental gradients. There is robust evidence showing patterns of ANPP along gradients of mean annual precipitation (MAP; Sala et al., 1988, 2012, Huxman et al., 2004). Yet, root:shoot ratios may be greater in drier ecosystems (Schenk and Jackson, 2002; Mokany et al., 2006; Wilcox et al., 2016, Hu et al., 2022), which may result in shallower relationships between MAP and total NPP. Biomass turnover is associated with τ_E and has been shown to be an important part of biogeochemical responses

https://doi.org/10.5194/bg-2022-164
Preprint. Discussion started: 18 August 2022

to changes in environmental conditions (De Kauwe et al., 2014), yet turnover of above and belowground plant biomass within a growing season is often difficult to measure empirically and is missing from many above- and belowground NPP field measurements.

Similar to NPP, there is evidence that respiration rates increase with MAP and MAT due to favorable soil conditions for decomposition (Bird et al., 1996, Carvalhais et al., 2014, Stielstra et al., 2015, Feng et al., 2018), leading to shorter τ_E in warm and wet ecosystems. Additionally, τ_E may be controlled by differences in microbial and fungal decomposer communities (Williams and Rice, 2007; García-Palacios et al., 2016). For example, You et al. (2014) found that the relative abundances of gram-negative bacteria, saprophytic fungi, and actinomycetes had strong impacts on C acquisition and soil organic matter loss in central China forest ecosystems. Currently, information is limited as to how these C input versus output relationships across ecosystems combine to impact X_C along climatic gradients, or how the difference between X_C and X_P (i.e., CSAT) varies.

In this study, we (a) assimilated C pool and flux data from six US grassland sites with a process-based ecosystem model (see methods for in depth description of the model) to estimate primary C inputs (NPP), τ_E, and X_C, and (b) measured X_P as the sum of soil and vegetative C to quantify what proportion of X_C was currently contained in each of these systems (C_{SAT}). We address the following questions and associated hypotheses:

1. How do NPP, τ_E, and X_P vary across gradients of MAP and MAT? We hypothesize that NPP should be primarily related to precipitation, due to strong water limitation in grasslands (Sala et al., 1988, Huxman et al., 2004), and τ_E will be related to both temperature and precipitation due to strong limitation of these factors on microbial activity.
2. Is X_P in any of these systems close to X_C?
3. How does C_{SAT} vary across these grasslands? As C_{SAT} is the distance between X_P and X_C and depends on both the time since disturbance and the rate at which X_C approaches X_P, we hypothesize that C_{SAT} will be less in cooler and drier ecosystems, since these environmental conditions promote slow growth and slow turnover. As such, these systems will take longer for X_C to approach X_P after perturbations.

Addressing these questions and hypotheses will provide an initial perspective on how much these key C attributes vary spatially, as well as identify regions and ecosystems that are vulnerable to C loss, and land areas that should be high priority for future research and management efforts.

https://doi.org/10.5194/bg-2022-164
Preprint. Discussion started: 18 August 2022

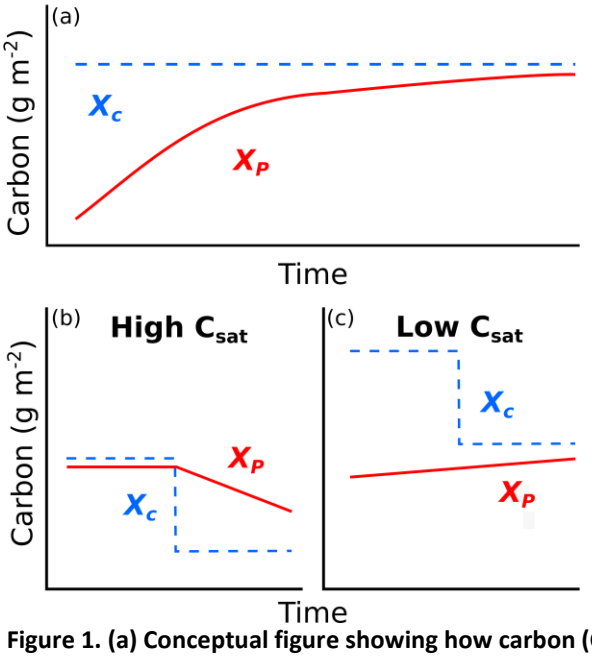

Figure 1. (a) Conceptual figure showing how carbon (C) changes through time to approach C storage capacity as a function of the difference between C storage at present (X_P) and C storage capacity (X_C). Changes in X_C (blue dashed lines in b-c) can be caused by alterations in net primary productivity or ecosystem C residence time. (b) Ecosystems that have X_P close to X_C are susceptible to C loss if environmental conditions cause reductions in X_C, while (c) ecosystems having X_P far below X_C may be buffered against C losses, at least in the short-term.

2. Methods

2.1 Site descriptions

We conducted this study at six US grassland sites spanning climatic gradients of mean annual precipitation (MAP) and mean annual temperature (MAT; Table 1). Data collection sites were set up and maintained as part of the Extreme Drought in Grasslands Experiment (EDGE), and represent the major grassland types within the central United States: desert grassland (SBK), shortgrass prairie (SBL, CPER), northern mixed grass prairie (HPG), southern mixed grass prairie (HAR), and tallgrass prairie (KNZ). All sites were ungrazed for >15 years before the start of data collection, and all sites except KNZ were not frequently burned. KNZ was burned annually to reflect common management in this region (Knapp et al. 1998, Freckleton et al. 2004). See Table 1 and Knapp et al. (2015) for more information about these sites.

https://doi.org/10.5194/bg-2022-164
Preprint. Discussion started: 18 August 2022

Table 1. Site characteristics of each of the six grassland sites in this study.

	Site characteristic	SBL	SBK	CPER	HPG	HAR	KNZ
Climate[a]	Grassland type	Shortgrass prairie	Desert grassland	Shortgrass prairie	Mixed-grass prairie	Mixed-grass prairie	Tallgrass prairie
	Mean annual precipitation (mm)	246	246	375	400	584	892
	Mean growing season precipitation (mm)[b]	163	163	293	303	426	652
	CV of growing season precipitation[b]	48.5	48.5	33.5	32.8	34.7	29.8
	Mean annual temperature (°C)	13.4	13.4	9.5	7.9	12.3	13.0
	Mean growing season temperature (°C)[b]	19.3	19.3	16.4	14.6	20.8	21.4
Soil	Bulk density (g cm^{-3})[c]	1.68	1.68	1.26	1.18	1.16	1.03
	Field capacity (% soil moisture)[d]	27	30	17	29	35	38
	Wilting point (% Soil moisture)[d]	7	5	5	10	16	15
Vegetation[e]	C_3 graminoid (%)	0	0	17.5	53.7	9.0	11.9
	C_4 graminoid (%)	48.7	52.0	54.0	27.0	68.9	77.0
	CAM (%)	22.8	0	6.6	0	0.4	0
	Forb (%)	24.2	44.86	19.2	12.5	19.6	8.4
	Woody (%)	3.4	2.3	1.9	5.9	1.2	2.5
	Perennial (%)	82.4	77.5	82.5	95.1	96.6	99.5
	Annual (%)	16.8	21.5	16.6	3.9	2.4	0.4

[a]Climate characteristics are from 1982-2012 weather data, obtained from Knapp et al. 2015
[b]Growing season was defined as April-September for CPER, HPG, HAR, and KNZ, and as April-October for SBL and SBK
[c]Bulk density data obtained from measurements taken at each site in 2015
[d]Estimated using hourly soil moisture data from 2012-2013 in SBL and SBK and from 2013-2015 in CPER, HPG, HAR, and KNZ
[e]Estimated from plant species composition measurements taken during the 2012-2013 growing seasons at SBL and SBK and during the 2014 growing season at CPER, HPG, HAR, and KNZ

2.2 Sampling design

For this study, we used measurements of aboveground net primary productivity (ANPP), belowground net primary productivity (BNPP), root standing crop biomass, vegetative litter biomass, soil C, volumetric soil moisture, soil temperature, soil CO^2 efflux, plant species abundance, soil bulk density, and hourly meteorological data. Most of these data were collected from control plots within the EDGE experimental infrastructure, which is a randomized block design having 10 blocks each containing three treatments: one control and two drought treatments; for the purposes of this study, we only use control data from the ten 6 m^2 control plots at each site. See Appendix C for details about sampling regimes.

https://doi.org/10.5194/bg-2022-164
Preprint. Discussion started: 18 August 2022

2.3 Estimating GPP and NPP

To generate gross primary productivity (GPP) and net primary productivity (NPP) estimates, we operated the grassland version of the Terrestrial Ecosystem Model (TECO; Weng and Luo, 2008; Shi et al., 2015), which has been shown to produce NEE estimates that match observations well in US grassland ecosystems (Shi et al., 2014). TECO is a process-based ecosystem model that has four major sub-models to simulate canopy photosynthesis, plant growth (allocation and phenology), soil water dynamics, and soil carbon turnover based on weather data and site level soil characteristics (Figure A1). To run the model, we used hourly air temperature, relative humidity, vapor pressure deficit, precipitation, and incident photosynthetically active radiation data from nearby weather stations (see Appendix C for additional details about collecting and cleaning meteorological data). GPP and NPP were generated for the main analyses in this paper using TECO for 2012-2014 at SBL and SBK, and for 2013-2015 at the other four sites. The mismatch in time frame among sites was due to data availability.

Formal model validation of the vegetation components of the model was conducted at each of the six sites. This was done by calibrating the model for each site based on measured above and belowground plant growth, soil texture, site-level field capacity and wilting point. Then, model spin-up of 500 years (all pools stabilized at each site between 200 and 400 years) was conducted and output from 2014-2017 was compared with observations at each site. Overall, cross-site mean primary production estimates from the model matched empirical observations very well (aboveground biomass R^2=0.99, belowground NPP R^2=0.94). Interannual variability in production from the model was less well correlated with empirical observations, although model predictions most often fell within one standard deviation of empirical observations. (See Appendix D for additional model validation discussion, figures, and tables).

2.4 Optimizing C submodel parameters

Within the C turnover submodel in TECO (Fig. A1), parameters for C turnover rates, C transfer rates, and environmental scalars (Table B1) were estimated for each site using data assimilation techniques (Xu et al., 2006; Shi et al., 2015). For optimization, we designated (1) six C turnover parameters associated with leaf, fine root, litter, fast SOM, slow SOM, and passive SOM carbon pools, (2) seven C transfer coefficients controlling the proportion of C turnover transferred to other C pools, and (3) two environmental scalars that control C turnover rates based on soil moisture and soil temperature (Table B1). Using a Markov Chain Monte-Carlo method with Metropolis-Hastings algorithm, we allowed these parameters to vary within biologically reasonable bounds with a step size of 15 over 4 chains of 360,000 iterations to optimize alignment of model output with ANPP, root standing crop, plant litter, soil C, and surface CO_2 efflux observations. Starting parameter values were obtained from previous studies (Xu et al., 2006, Shi et al., 2015, Zhou et al., 2012)(Table B1). Gelman-Rubin (GR) values were mostly < 1.1, with the exception of a few parameters having 1.2 or 1.3 GR values at HPG and HAR (Table B2). All parameters where GR values were high did not converge and drifted slowly over iterations. This resulted in estimates of these parameters close to the midpoint of the parameter bounds, and large uncertainty. To account for this,

https://doi.org/10.5194/bg-2022-164
Preprint. Discussion started: 18 August 2022

uncertainty in parameter estimates was incorporated into τ_E estimates via bootstrapping methods (see below). Cross-correlations were calculated for all parameters at each site (Table B3). Maximum likelihood estimates (MLE) and uncertainty (95% confidence intervals) were calculated for each parameter at each site by assessing normal, log-normal, or Weibull distributions depending on the magnitude and direction of skew (Fig. A2-A4, Table B2).

2.5 Estimating τ_E, X_C and C_{SAT}

We calculated ecosystem C residence time (τ_E) following Luo et al. (2017):

$$\tau_E = (A\xi(t)K)^{-1}B \quad (1)$$

, where ξ(t) represents the environmental scalar determined by soil moisture and soil temperature at time step *t*, *A* is a matrix of C transfer coefficients, *K* is a 6x6 diagonal matrix representing rates of C loss per day from each of the six C pools, and B is a 6x1 matrix representing the allocation fractions of GPP to each of the six C pools:

$$\xi(t) = F_T(t)F_W(t); \quad (2)$$

$$A = \begin{pmatrix} -1 & 0 & 0 & 0 & 0 & 0 \\ 0 & -1 & 0 & 0 & 0 & 0 \\ 1 & 1 & -1 & 0 & 0 & 0 \\ 0 & 0 & f_{4\leftarrow3} & -1 & f_{4\leftarrow5} & f_{4\leftarrow6} \\ 0 & 0 & f_{5\leftarrow3} & f_{5\leftarrow4} & -1 & 0 \\ 0 & 0 & 0 & f_{6\leftarrow4} & f_{6\leftarrow5} & -1 \end{pmatrix}; \quad (3)$$

$$K = \begin{pmatrix} c_1 & 0 & 0 & 0 & 0 & 0 \\ 0 & c_2 & 0 & 0 & 0 & 0 \\ 0 & 0 & c_3 & 0 & 0 & 0 \\ 0 & 0 & 0 & c_4 & 0 & 0 \\ 0 & 0 & 0 & 0 & c_5 & 0 \\ 0 & 0 & 0 & 0 & 0 & c_6 \end{pmatrix} \quad (4)$$

$$B = (X_A, X_B, 0, 0, 0, 0) \quad (5)$$

In Eqn. 2, F_T is the effect of soil temperature on microbial decomposition rates at time *t*: $Ft(t) = 0.58Q_{10}^{(T(T)-10)/10}$, where Q_{10} is a constant parameter and *T* is soil temperature. F_W is the potential effect of soil water content on microbial decomposition rates at time *t*: $F_W(t) = 1 - 5(mscut-W(t))$, where *mscut* is a constant parameter representing the soil water content (*W*) below which microbial decomposition becomes limited. If *W* is greater than *mscut*, $F_W = 1$. The impact of F_T and *Fw* scalars on ξ are dependent on one another (i.e. F_W will limit ξ in dry conditions even if soil temperatures lead to a large F_T). In Eqn. 3, $f_{i\leftarrow}$

https://doi.org/10.5194/bg-2022-164
Preprint. Discussion started: 18 August 2022

$_j$ represents the fractions of C turnover entering pool *i* pool from pool *j*. In Eqn. 4, $c_{1\text{-}6}$ represents the amount of carbon lost from pools 1-6 per day, where pool 1=aboveground plant biomass, 2=belowground plant biomass, 3=fine litter biomass, 4=active (fast) soil organic matter (SOM), 5=slow SOM, 6=passive SOM. In Eqn. 5, X_A and X_B are the fractions of GPP allocated to aboveground and belowground vegetative pools, respectively. For each site, X_A and X_B were estimated from observed ANPP:BNPP ratios, and data assimilation was used to estimate $c_{1\text{-}6}$, $f_{i \leftarrow j}$, Q_{10}, and *mscut* parameters. To generate uncertainty surrounding τ_E, we bootstrapped 1000 parameter sets from the Markov chain Monte Carlo (MCMC) and obtained the MLE and 95% confidence intervals from the resulting distribution of τ_E estimates.

C capacity (X_C) was calculated following Luo et al. (2017) as:

$$X_C = NPP \cdot \tau_E \quad (6)$$

, where NPP is net primary productivity of a site, obtained via TECO simulations, and τ_E is the MLE of the distribution of bootstrapped τ_E values. At KNZ, NPP in Eqn. 6 consisted only of the belowground component because annual fire removes all aboveground plant material each spring. We recognize the limitation of using three years of NPP data to estimate X_C, yet we believe it is important that NPP and τ_E estimates are derived from the same time periods, and the data necessary to estimate τ_E were only available for three years. Weather within the three focal years was comparable to long-term averages at most of the sites (Fig. A5), although precipitation was greater than the long-term average at HPG, lower than the long-term average at HAR, and air temperatures were warmer at SBK and SBL in 2012-2014. Standard deviation of X_C (C_{sd}) was calculated as

$$C_{sd} = X_C \sqrt{\left(\frac{\sigma_{NPP}}{NPP}\right)^2 + \left(\frac{\sigma_{\tau E}}{\tau_E}\right)^2} \quad (7)$$

, where σ_{NPP} is the standard deviation of NPP across years, and $\sigma_{\tau E}$ is the standard deviation of the 1000 bootstrapped iterations of τ_E. The level of C saturation (C_{SAT}) represents the percentage of X_C that is represented by X_P, calculated as

$$C_{SAT} = \frac{C_S + C_A + C_B}{X_C} \quad (8)$$

, where C_S is the amount of C in the soil, C_A is the observed aboveground biomass * 0.45, and C_B is the observed root biomass * 0.45. We ran variance partitioning to determine the amount of cross-site variance in X_C that was driven by variation in NPP versus τ_E. Since only BNPP was incorporated into the X_C calculation for KNZ, we performed this analysis both with and without KNZ (Fig. A6).

For Eqn. 8, soil C measurements from 0-10 cm in the soil were extrapolated to 0-20 cm to match up with the depth of BNPP observed and used to calibrate the model. This was done by extracting soil C data along a depth profile (0 to >1 m depth)

https://doi.org/10.5194/bg-2022-164
Preprint. Discussion started: 18 August 2022

from the international soil carbon network (ISCN; Nave et al 2017) in nearby areas having similar cover types and land management regimes (Table B4). These depth profiles were used to calculate the proportion of soil C across depths using a beta distribution described by Jobággy and Jackson (2000)(Fig. A7). Then, soil C measurements from 0-10 cm were extrapolated along this curve to estimate the amount of soil C from 0-20 cm (Fig. A7).

2.6 Sensitivity analyses

For each parameter used to calculate τ_E, we varied the parameter while keeping all other parameters constant at their MLE and recorded the resulting τ_E. We did this for 20 intervals ranging from the minimum to maximum parameter values shown in Table B1. We also wished to determine the impact of each parameter value at each site as estimated via data assimilation. To this end, we shifted each parameter from its default value (Table B1) to the MLE value obtained from data assimilation (Table B2) – holding all other parameters at their default values – and observed the resulting effect on τ_E (Fig. 3g-l).

2.7 Statistical analyses

NPP, τ_E, X_P (soil + vegetative C), MAP, and MAT were all normalized across sites by the cross-site means for regression analysis to allow for slope values to be comparable. Standardized NPP, τ_E, and X_P values were compared across sites with standardized MAP and MAT using linear regression. Additional site-level characteristics (Bulk density, grass:forb, C_3:C_4, Annual species abundance) were combined with climate data using partial regression and adjusted R^2 values were assessed to test whether site-level climate-NPP or climate-τ_E relationships were being driven by other site-characteristics (vegan package, Oksanen et al. 2016). Bayesian data assimilation was run using a custom script; linear models were run with the lm() function. All analyses were conducted in R (R core team, 2022).

3 Results

3.1 Net primary productivity (NPP) and X_P

Estimates of NPP varied across sites from 45.3 g C m^{-2} yr^{-1} at SBL to 400.2 g C m^{-2} yr^{-1} at KNZ (Table 2). The standardized full NPP model (NPP ~ MAP + MAT) was significant ($F_{2,3}$=63.8, P<0.01) and explained 96% of the cross-site variation in NPP estimates (Adj. R^2 = 0.96). Within the model, MAP was strongly correlated with NPP across sites ($F_{1,3}$=123.7, P<0.01), while the relationship with MAT was not significant ($F_{1,3}$=0.58, P=0.50)(Fig. 2). The non-standardized relationship between MAP and NPP was of the form $NPP = 0.53*MAP - 51.4$. We looked for collinearity of MAP with soil bulk density, grass:forb, C_3:C_4, and annual species abundance using partial regression analysis. We found that MAP was still a significant and strong predictor of NPP when these other variables were accounted for (Table B5). Similarly, we found a weak positive relationship between X_P and MAP ($F_{1,3}$=6.59, P=0.08, Adj. R^2=0.54), and no relationship between MAT and X_P (Fig. 2). The non-standardized relationship between MAP and X_P was of the form $X_P = 767.4 + 4.0*MAP$.

https://doi.org/10.5194/bg-2022-164
Preprint. Discussion started: 18 August 2022

Table 2. Estimates of NPP and ecosystem carbon residence time at all six sites. Uncertainty for ecosystem carbon residence time is propagated from parameter uncertainty. NPP standard deviation (σ) represents variance through time. See Table 1 for site details.

Site	τ_E (years)	$q_{2.5\text{-}97.5}$	$q_{5\text{-}95}$	$q_{25\text{-}75}$	NPP (g C m^{-2})	NPP σ (g C m^{-2})
SBL	26.74	6.86-104.27	8.53-83.78	16.74-42.71	45.30637	15.31988
SBK	26.59	13.47-52.46	15.03-47.03	21.04-33.59	67.74404	27.54944
CPER	54.24	18.02-163.25	21.51-136.75	37.12-79.25	143.5631	25.00492
HPG	52.44	25.82-106.49	28.94-95.03	41.09-66.91	157.5499	65.17631
HAR	53.08	19.88-141.75	23.28-121.04	37.85-74.43	173.2585	31.82541
KNZ	27.76	10.23-75.31	12.01-64.14	19.69-39.13	400.2068	140.9756

3.2 Ecosystem carbon residence time (τ_E)

Estimates of τ_E ranged across sites from 26.6 years in SBK to 54.2 years in CPER (Table 2). The standardized full τ_E model (τ_E ~ MAP + MAT) was less robust than that of NPP ($F_{2,3}$=3.3, P=0.18). Within the full model, MAP was not correlated with τ_E across sites ($F_{1,3}$=0.13, P=0.74), while the relationship with MAT was only significant at α=0.1 ($F_{1,3}$=6.57, P=0.08)(Fig. 2b). The non-standardized relationship between MAT and τ_E was of the form τ_E = -3.6**MAT* + 81.6. Based on partial regression, underlying relationships with other site-based variables were not driving the relationship between MAT and τ_E (Table B5).

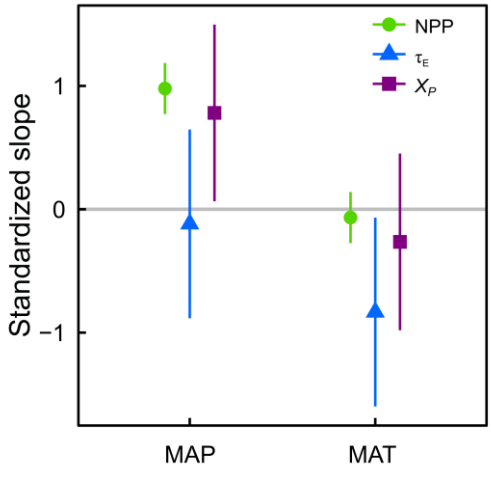

Figure 2. Slopes between standardized net primary productivity (NPP), ecosystem C residence time (τ_E), or X_P and standardized mean annual precipitation (MAP) and mean annual temperature (MAT). Error bars represent 90% confidence intervals.

https://doi.org/10.5194/bg-2022-164
Preprint. Discussion started: 18 August 2022


Biogeosciences Discussions Open Access EGU

3.3 Soil moisture and temperature effects on τ_E

All sites exhibited a cyclical pattern of soil moisture and temperature effects on C turnover rates (denoted ξ), with higher ξ during the growing season due to warmer temperatures (Fig. 3 black lines). ξ during the growing season was > 1 for all sites except CPER, meaning that C turnover rates were increased in the data driven model, rather than limited by soil conditions. At SBL and SBK (Fig. 3a,b), temperature constraints (F_T; Fig. 3 dashed orange lines) on ξ were > 1 for much of the growing season, yet ξ was limited by soil moisture constraints (F_W; Fig. 3 dotted blue lines) outside of the monsoonal season. Only when monsoonal rains removed soil moisture limitations did ξ generally persist above one. At CPER (Fig. 3c), ξ was not limited by F_W. Yet, F_T was < 1 throughout the year due to the low Q_{10} value estimated for CPER (Table B2). F_T was much greater than one during the growing season at both the mixed grass and tallgrass prairie sites (Fig. d-f), but F_W limited ξ at both mixed grass prairies. ξ was high at KNZ due to a lack of F_W effect at the site, which was a result of both high soil moisture content throughout the growing season, and a relatively low estimated *mscut* parameter value (Table B2).

https://doi.org/10.5194/bg-2022-164
Preprint. Discussion started: 18 August 2022

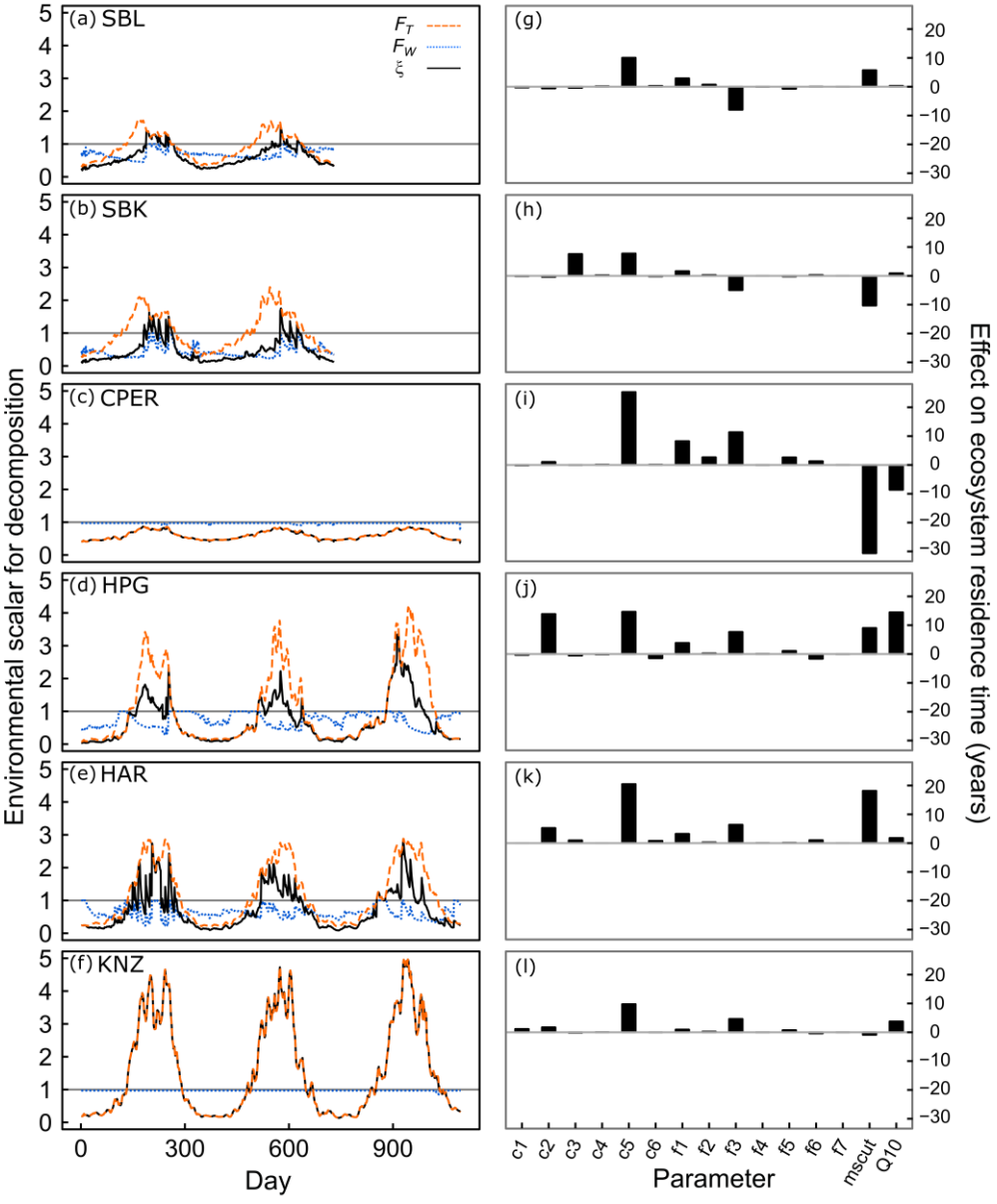

Figure 3. Environmental scalars for decomposition rates at six grassland sites (a-f) and impact of individual parameter estimates on ecosystem carbon residence time (g-l). In a-f, values less than 1 represent soil conditions limiting decomposition while values greater than 1 represent acceleration of decomposition due to soil conditions. Dashed orange lines represent the temperature scaling effect (F_T) – based on the site-estimated value of the Q_{10} parameter and daily soil temperature data. Dotted blue lines represent the moisture scaling effect (F_W), which is based on the site-estimated value of the *mscut* parameter and daily soil moisture data. Black solid lines represent the product of the temperature and moisture scalars (ξ), which is the overall environmental scalar that controls decomposition rates in the model. In g-l, parameters were shifted one at a time from their mean parameter space (baseline parameter) to the parameter estimates obtained from data assimilation, and the resulting effect on ecosystem carbon residence time is

https://doi.org/10.5194/bg-2022-164
Preprint. Discussion started: 18 August 2022

shown. This represents the inherent effect of each model parameter on τ_E independent from soil moisture or temperature. Panels correspond to different sites: a,g=Sevilleta National Wildlife Refuge blue grama grassland; b,h=Sevilleta National Wildlife Refuge black grama grassland; c,i=Central Plains Experimental Range; d,j=High Plains Grasslands Research Station; e,k=Hays Agricultural Research Center; f,l=Konza Prairie Biological Station. Transfer parameters (*fx←y*) dictate the proportion of C turnover in pool *y* transferring to pool *x*: f1=f4←3; f2=f5←3; f3=f5←4; f4=f6←4; f5=f4←5; f6=f6←5; f7=f4←6.

3.4 Parameter effects on τ_E

We then performed two sensitivity analyses to (1) identify variables in the model with potential to contribute the most to τ_E (Fig. 4), and (2) quantify the actual effect of various C turnover and C transfer variables on τ_E as estimated by data assimilation at each site (Fig. 3). These sensitivity analyses simulated τ_E under a range of parameter values while incorporating daily soil temperature and moisture measurements from each site. We found that C turnover rates of the slow and passive SOM pools had the potential to have the greatest impacts on ecosystem carbon residence time, suggesting the importance of C sequestration in these pools for maintaining C stocks (Figure 4). The *mscut* parameter was potentially important in determining ecosystem carbon residence time in our sensitivity analysis, and the effect increased exponentially until reaching ca. field capacity at each site. In the drier sites (SBL, SBK, and CPER), the effect started to increase rapidly around 10-15% volumetric soil moisture. The steep increase began at higher soil moisture levels (20-25%) at the more mesic sites (HPG, HAR, KNZ). At the warmer sites (SBL, SBK, KNZ), Q_{10} had less potential to alter τ_E, unless Q_{10} was very low (ca. 1). Interestingly, higher Q_{10} values had the potential to increase τ_E at the cooler sites (CPER, HPG). Although Q_{10} is generally positively related with C turnover, the form of the Q_{10} relationship is such that, although lower Q_{10} values result in slower turnover rates at high soil temperatures, they also result in higher turnover rates under cooler temperatures due to their shallower slope. As such, this can lead to a positive relationship between Q_{10} values and τ_E at cooler sites.

When we applied the estimated parameters to these sensitivity curves to estimate the actual effect of individual parameters on the τ_E estimates (Fig. 3 right panels), we found that turnover rates of the slow SOM pool increased τ_E greatly compared with starting parameters across all sites (+8 to +25 years). Root turnover had a substantial effect on τ_E at HPG (+14 years) and HAR (+5 years). The transfer proportion from fast SOM to slow SOM had a positive effect on τ_E at CPER, HPG, HAR, and KNZ (+5 to +11 years), and a negative effect on τ_E at SBL and SBK (-5 to -8 years). *mscut* had opposite effects on τ_E for SBL (+6 years) than SBK (-10 years), while Q_{10} had minimal effects at both sites. *mscut* and Q_{10} had strong negative effects on τ_E at CPER (-31 years and -9 years, respectively), likely due to particularly low *mscut* and Q_{10} estimated for that site (Fig. A4) and strong potential for impact of these parameters at CPER (Fig. 3). At the other cool site, HPG, both *mscut* and Q_{10} increased τ_E (+9 and +14 years, respectively). At HAR, a high *mscut* estimate increased τ_E (+18 years), suggesting that C turnover at this site may be particularly sensitive to soil moisture. Q_{10} estimated at HAR had minimal impact. *mscut*

https://doi.org/10.5194/bg-2022-164
Preprint. Discussion started: 18 August 2022

Biogeosciences Discussions Open Access EGU

and Q_{10} estimates at KNZ had small impacts on τ_E (-1 and +4 years, respectively, Fig. 3).

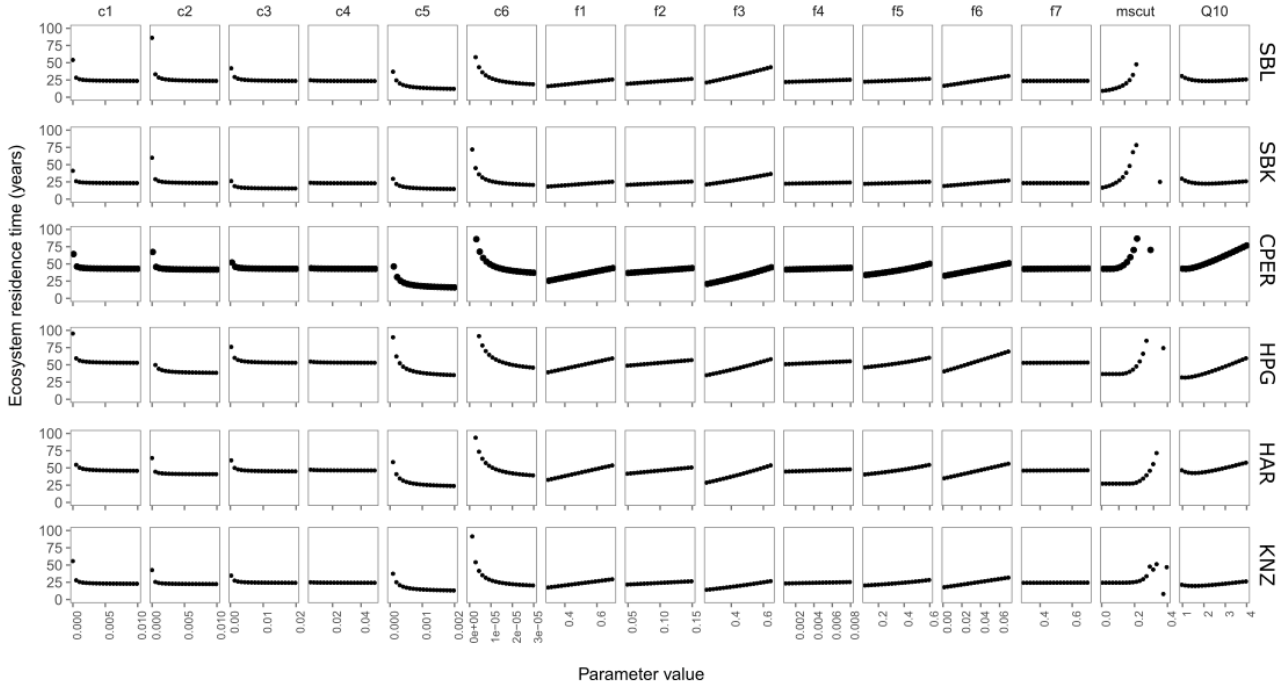

Figure 4. Results from sensitivity analysis where ecosystem carbon residence time was calculated when altering one parameter value at a time. Rows of panels correspond to different sites with: SBL= Blue grama dominated site at the Sevilleta National Wildlife Refuge; SBK= Black grama dominated site at the Sevilleta National Wildlife Refuge; CPER=central plains experimental range; HPG=High Plains Grassland Research Station; HAR=Hays Agricultural Research Station; KNZ=Konza Prairie Biological Station. Ecosystem carbon residence time was often very high at very extreme parameter values so the y axis was set for clarity. Transfer parameters (f1-7) are as in Fig. 3.

3.5 Carbon capacity (X_C) and carbon saturation (C_{SAT})

Finally, we used NPP and τ_E estimates to calculate X_C. Cross-site variation of NPP and τ_E were both important for determining X_C across the six grassland sites (Fig. A6), which varied from as little as 1211 g m^{-2} in SBL to as much as 9196 g m^{-2} in HAR (Fig. 5). We estimated C_{SAT} as the percentage of X_C made up by total ecosystem C. In the two hot and dry sites (SBL and SBK), we found that X_C was relatively small and less than total system carbon (Fig. 5), resulting in high C_{SAT} values (SBL= 184% and SBK = 126%). The cooler and/or wetter sites all had much higher X_C values and ecosystem C (X_P) below X_C; C_{SAT} values for these sites were: CPER 34%, HPG 61%, and HAR 66% saturated. The exception to this was KNZ, the most mesic but frequently burned site with a C_{SAT} value of 137% (Fig. 5 inset).

https://doi.org/10.5194/bg-2022-164
Preprint. Discussion started: 18 August 2022

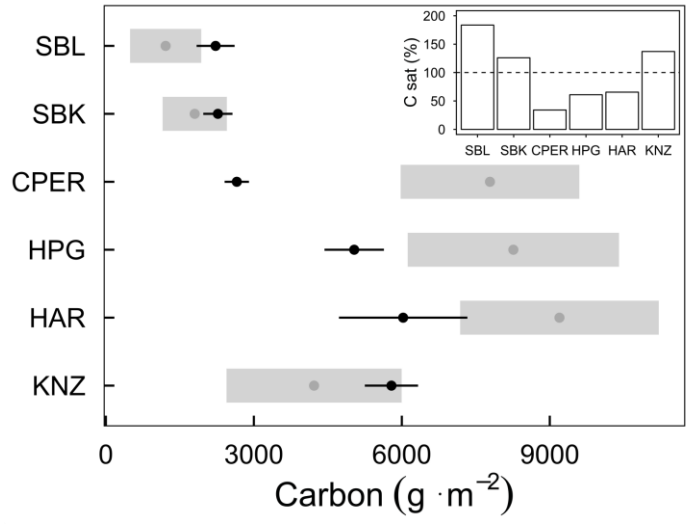

Figure 5. Ecosystem carbon capacity (X_C; grey points) and ecosystem carbon content (X_P; black points) in six grassland ecosystems. X_P was calculated using estimates of soil C from 0-20 cm + aboveground and belowground vegetative C. Black error bars and grey rectangles represent 1 standard deviation around the mean. Inset: Carbon saturation is the percent of X_P represented by X_C, where 100% (dotted line) represents equilibrium (X_P = X_C).

4. Discussion

Our findings provide insights for the three questions we posed at the start of this study: (1) How do NPP, τ_E, and X_P vary across gradients of MAP and MAT? (2) Is X_P in any of these systems close to X_C? and (3) How does the level of C_{SAT} vary across these grasslands? Related to our first question, we found general support for our hypothesis, in that NPP and X_P exhibited positive relationships with MAP, while τ_E estimates indicated slower C turnover in cooler sites. The cross-site pattern of τ_E was driven by both differences in edaphic environments (soil moisture and soil temperature) as well as inherent differences in turnover rates, which may be indicative of biological or physical differences across sites (Baisden et al., 2013, Mathieu et al., 2015, Doetterl et al., 2015, Zhao et al., 2021). Related to our second and third questions, we found that three of these grasslands had particularly high C_{SAT} values, indicating vulnerability to C change in the future and a limited ability of these systems to be long-term C sinks. Two of these three grasslands were in hot, dry climates where C turnover rates were high and C inputs through NPP low. The third grassland (KNZ) was the most mesic and had the highest levels of productivity, yet annual burning at KNZ increased C_{SAT} substantially. Below, we discuss these findings in more detail.

4.1 Relationships of NPP, τ_E, and X_P with climate

Abundant research exists showing spatial relationships between ANPP and climate. Sala et al. (1988) was able to explain 90% of the cross-site variation in averaged ANPP with mean annual precipitation across the Great Plains. Yet, total NPP (ANPP + BNPP) is a better determinant of C processes due to large contributions of root C to soil pools (Sulzman et al.,

https://doi.org/10.5194/bg-2022-164
Preprint. Discussion started: 18 August 2022

2005; Guzman and Al-Kaisi, 2010; Leppälammi-Kujansuu et al., 2014). A potential reason why BNPP and total NPP relationships with climate may be less clear than ANPP relationships is that, in wetter ecosystems, plants tend to allocate less carbohydrates to roots and more to aboveground material (Schenk and Jackson, 2002, Mokany et al., 2006, Wilcox et al., 2016, Hu et al., 2022). This pattern results in a weaker relationship between MAP and NPP than predicted by ANPP-MAP relationships since BNPP is proportionally greater in drier ecosystems. Indeed, we found some evidence for this from our model simulations – the slope of the BNPP-MAP regression (0.24 +/- 0.03, slope estimate +/- standard error) was shallower than the slope of the ANPP-MAP regression (0.29 +/- 0.02, Fig. A8). Also, differences in functional composition of vegetation may drive site differences in root:shoot (e.g., annual versus perennial species). Despite the additional uncertainty associated with total NPP, we found that MAP was a strong predictor of total NPP across the six grassland sites (Fig. 2a).

We hypothesized that τ_E should be greater in (1) cooler systems due to lower soil temperatures and shorter growing seasons and (2) drier systems due to moisture limitations on microbial activity. Previous studies examining patterns of ecosystem C residence time have found relationships of varying strengths with climate or latitude (Bird et al., 1996, Chen et al., 2013, Carvalhais et al., 2014, Moore et al., 2018), biome type (Zhou and Luo, 2008), soil properties (Telles et al., 2003), and land use change (Wu et al., 2020). Yet, there is much uncertainty associated with trends in τ_E (Friend et al., 2014). We found that MAT was a better predictor than MAP for τ_E across the six grasslands we examined (Fig. 2b). This was especially apparent at the two hottest sites (SBL and SBK), as they had particularly short τ_E, likely due to strong C limitation of microbes at these sites and high abundances of fungal decomposers that efficiently break down recalcitrant C (Collins et al., 2008, Sinsabaugh et al., 2008). Additionally, intense wet-dry cycles (Fierer and Schimel, 2002), soil burial (Brandt et al., 2010), and photo-degradation (Austin and Vivanco, 2006, Parton et al., 2007) have all been shown to be important accelerators of decomposition rates in arid systems and may be contributing to the low τ_E in these grasslands. As soil C is a function of both NPP and τ_E, it makes sense that the stronger relationship of the two is the one that is best related to X_P. We found that the best variable related to X_P was MAP (Fig. 2), so soil C may be more sensitive to changes in precipitation versus temperature in U.S. grassland systems. This corresponds with observational studies (Saiz et al., 2012) as well as meta-analysis findings of stronger moisture than temperature effects on net ecosystem exchange (Wu et al., 2011).

4.2 Effects of soil environment versus inherent site differences on C turnover rates

τ_E is directly related to various C turnover rates within an ecosystem (Luo et al., 2017). These turnover rates can be driven by favorability of soil environments for microbial activity (Bird et al., 1996, Carvalhais et al., 2014, Stielstra et al., 2015) or by differences in soil types and microbial communities (Williams and Rice, 2007, Collins et al., 2008, Garcia-Palacios et al., 2016, Bhattacharyya et al., 2022). With our approach, we were able to model the effect of temperature and moisture on turnover rates while accounting for site-level differences in how sensitive turnover is to soil moisture and temperature (through data-assimilation estimation of Q_{10} and *mscut* parameters; Fig. S5). At four of the six grasslands, both moisture and temperature had strong effects on C turnover during the growing season (Fig. 3a,b,d,e), which corresponds to well-known

https://doi.org/10.5194/bg-2022-164
Preprint. Discussion started: 18 August 2022

moisture and temperature controls on microbial activity (Bell et al., 2008). However, in the mesic tallgrass prairie (KNZ) and Colorado shortgrass prairie (CPER), we found moisture limitation on C turnover was minimal (Fig. 3c,f). At KNZ, this was likely due to relatively high soil moisture levels throughout the growing season (Table B6). In conjunction with soil temperatures optimal for microbial activity, this resulted in high C turnover rates throughout the growing season at KNZ (Fig. 3f) and low overall ecosystem C residence times.

Alternately, soils at CPER are coarse (Table B1) and become very dry during later months of the growing season, yet C turnover was not limited by moisture at the site within the data driven model. The may be due to low sensitivity of microbial communities to soil moisture at the site. The *mscut* parameter in TECO represents the soil moisture level at which C turnover – and by inference, soil microbial activity – in the system becomes limited. Because we were able to use daily soil CO_2 fluxes that were directly linked with soil temperature and soil moisture data for at least two years at each site, our estimates of *mscut* (and Q_{10}) parameters were remarkably well constrained (Fig. A4; Table B2). The estimate of the *mscut* parameter at CPER was 7%, the lowest of all six sites. This means that when volumetric soil moisture is above 7%, microbial activity is not restricted by soil moisture in the model. Soils at CPER during the growing season (June-Sept) were the driest of all the sites, having an average soil volumetric water content (VWC) of 11% (Table B6). Additionally, the site having the second driest soils (12% VWC – SBK) also had a low *mscut* estimate (Fig. A4). This raises the interesting possibility that ecosystems with drier soils have microbial communities adapted to low water conditions, which would result in C turnover rates persisting even in relatively xeric conditions. If it is the case that C turnover is less responsive to altered soil moisture, this could result in mismatches between responses of C inputs versus outputs under altered precipitation regimes, since NPP has been shown to be highly sensitive to precipitation in more arid ecosystems (Huxman et al., 2004, Sala et al., 2012, Maurer et al., 2020).

4.3 Patterns of C saturation

Three of the grasslands we assessed had large gaps between current X_P and X_C (CPER, HPG, and HAR; Fig. 5). Similar to forests acting as long-term C sinks during recovery from clear cutting regimes (Pan et al. 2011), it is possible that these cooler and/or wetter grassland ecosystems will act as C sinks due to long-term agricultural or other land-management legacies (Smith, 2014). These systems may be buffered against C losses if environmental changes occur, at least in the short-term. Alternately, the two hot and dry ecosystems showed high C_{SAT} levels (Fig. 4), which corresponds with previous work at the SBK site showing this system is often a C source (Petrie et al., 2015). High C_{SAT} in these systems may also lead to C losses in the future, especially if global changes reduce either NPP or τ_E, and C in these systems may be particularly vulnerable to drought due to high sensitivity of NPP in these systems (Huxman et al., 2004, Thomey et al., 2011, Sala et al., 2012).

https://doi.org/10.5194/bg-2022-164
Preprint. Discussion started: 18 August 2022

KNZ also had short τ_E, but it had the highest NPP value as well (Table 2), which should have resulted in a high X_C. Yet, this system is burned annually in the spring, a common management practice in this region (Knapp et al., 1998; Freckleton, 2004). This minimizes the amount of aboveground tissue that is incorporated into the soil due to volatilization of C to the atmosphere (Seastedt, 1988), although some C is deposited at pyrogenic C in this system (Soong and Contrufo, 2015). Despite these annual losses, X_C is still relatively close to X_P, perhaps due to increased root production under frequent fire regimes (Johnson and Matchett, 2001). This may be one reason that research in this ecosystem has found that soil C is resistant to altered environmental conditions despite frequent fire (Wilcox et al., 2016).

Our estimates of both X_C and X_P did not include measurements of C below 20 cm in the soil. In many grasslands, C fluxes aboveground and in shallow soil layers are more likely to change under global change scenarios than deeper soils because: (1) the proportion of root production of soil organic C and microbial activity are typically greatest within shallow soil layers (Jackson et al., 1996, Jobággy and Jackson, 2000, Blume et al., 2002, Taylor et al., 2002), and (2) altered air temperature is more likely to impact soil temperatures in shallow soils versus deeper soils. However, deeper C represents an additional store of C in many ecosystems and may stabilize C in ecosystems where C inputs by roots at depth are frequent, such as savanna and shrubland ecosystems. Additionally, soil microbial communities differ markedly in deeper soil layers than shallow layers (Fierer et al., 2003), so turnover rates across these systems may be quite different for deeper soils.

5 Conclusions

Here we used a recently developed metric, carbon capacity (X_C), to assess potential future trajectories of ecosystem C across six grasslands in the US Great Plains, and to identify grasslands that may be vulnerable to C loss under future global change scenarios. We showed that hot and dry grasslands had C contents greater than X_C, indicating the vulnerability of C in these system to loss. As arid ecosystems have been shown to be key components of the global C cycle due to their broad spatial extent (Poulter et al., 2014), understanding how NPP and ecosystem carbon residence times respond to alterations in environmental conditions in these ecosystems is vital for assessing future global C budgets. Additionally, the effect of frequent burning on C_{SAT} suggests that land management practices that remove aboveground biomass may result in reduced capacity for these systems to be C sinks into the future. However, the effects of disturbances such as fire are complex and often are critical to maintaining ecosystem structure so holistic consideration of all effects is important for management decisions. Because anthropogenic and climate effects on ecosystems are global and ubiquitous, considerations of how land management and environmental impacts interact to control ecosystem functioning are critical for land management and policy decisions related to C sequestration.

Appendices:

Appendix A. Supplemental Figures A1-A8

Appendix B. Supplemental Tables B1-B6

https://doi.org/10.5194/bg-2022-164
Preprint. Discussion started: 18 August 2022

Appendix C. Supplemental text describing data collection and cleaning methods

Appendix D. Model evaluation text, Table D1, Figures D1-D2

https://doi.org/10.5194/bg-2022-164
Preprint. Discussion started: 18 August 2022

Appendix A. Supplemental figures A1-A8

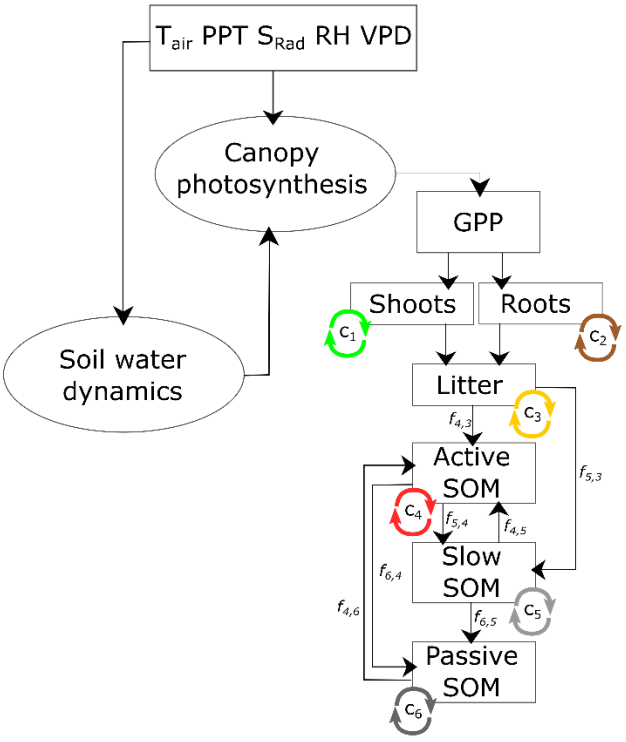

Figure A1. Schematic of the submodels making up the Terrestrial Ecosystem model. Canopy photosynthesis is determined by hourly meteorological information through direct impacts (e.g., vapor pressure deficit) and alterations to soil environmental conditions (e.g., soil moisture and temperature). GPP is estimated from the canopy photosynthesis model. Carbon from the canopy model is transferred to different components of vegetation, which is summed over an annual time step to estimate NPP (GPP – autotrophic respiration). See Weng and Luo (2008) for additional details of the model. The soil C model incorporates turnover rates for aboveground vegetation (c_1), roots (c_2), litter (c_3), active SOM (c_4), slow SOM (c_5), and passive SOM (c_6). Turnover rates are modified by an environmental scalar (τ) at each time step. The proportion of C transferred between pools are controlled by the $f_{i,j}$ parameters, which represent the proportion of C turnover transferred from C pool *j* to pool *i*, with the pool numbers corresponding to the subscripts by the C turnover parameters.

https://doi.org/10.5194/bg-2022-164
Preprint. Discussion started: 18 August 2022

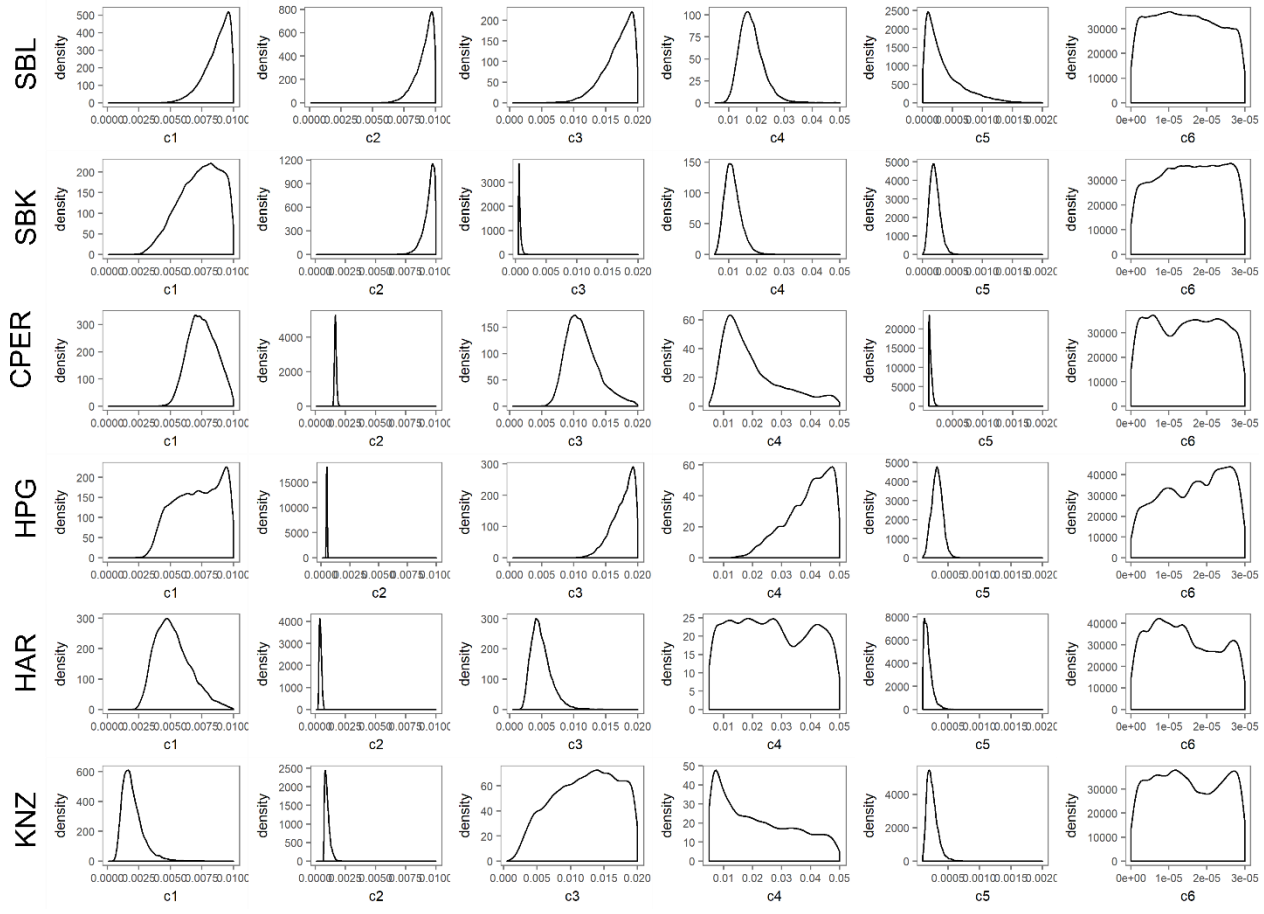

Figure A2. Density plots showing distribution of estimated carbon turnover parameters (columns) using data assimilation techniques with a 6 pool carbon model and 4-5 data sets describing carbon pools and fluxes at each of the six sites (rows). Densities reflect 4 chains of 360k simulations each, with the first 20k simulations removed. SBL= Blue grama dominated site at the Sevilleta National Wildlife Refuge; SBK= Black grama dominated site at the Sevilleta National Wildlife Refuge; CPER=central plains experimental range; HPG=High Plains Grassland Research Station; HAR=Hays Agricultural Research Station; KNZ=Konza Prairie Biological Station. All carbon turnover parameters are in units of gC lost gC^{-1} day^{-1}: c1=leaf turnover; c2=root turnover; c3=litter turnover; c4=fast SOM turnover; c5=slow SOM turnover; c6=passive SOM turnover.

https://doi.org/10.5194/bg-2022-164
Preprint. Discussion started: 18 August 2022

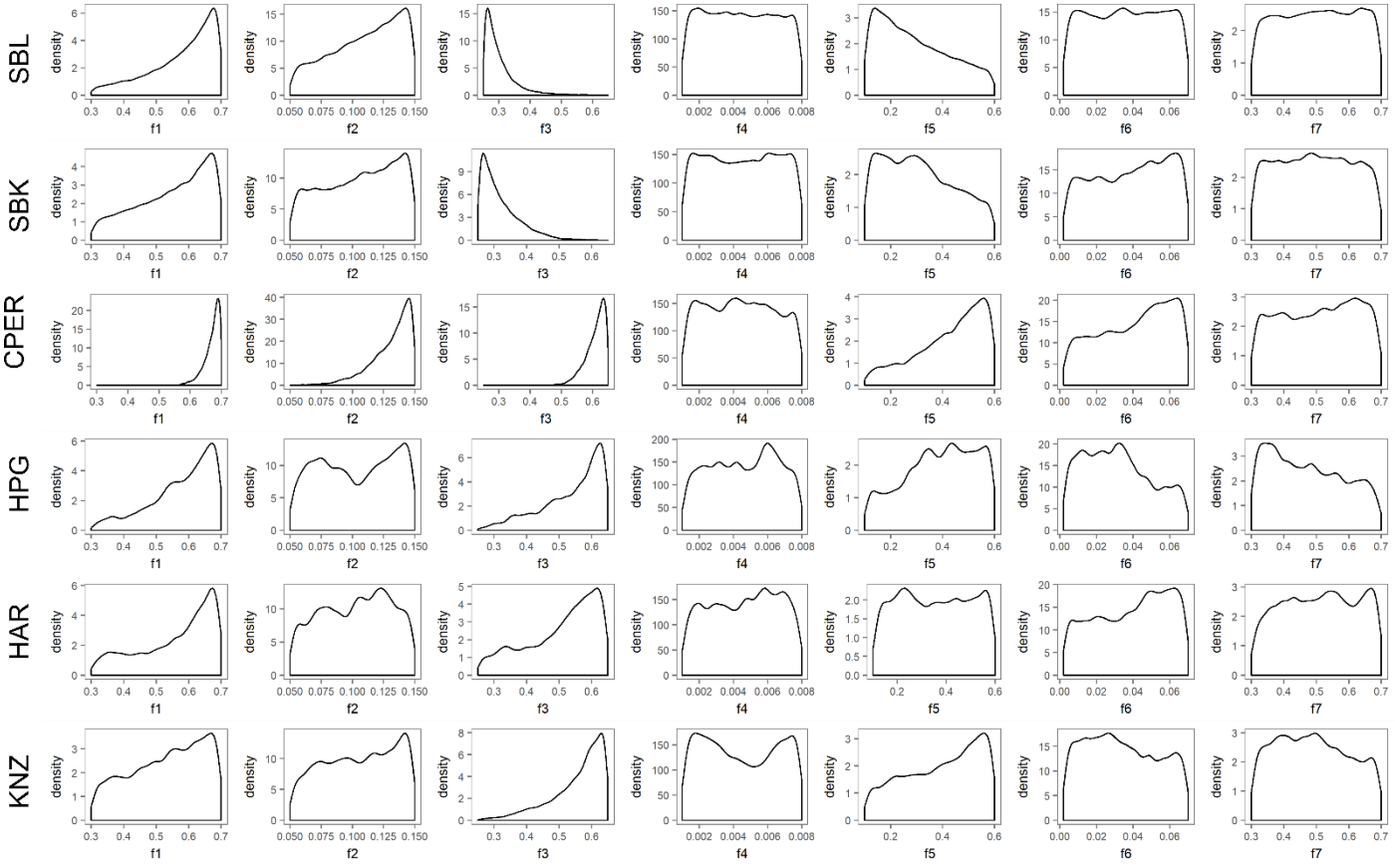

Figure A3. Density plots showing distribution of estimated carbon transfer parameters (columns) using data assimilation techniques with a 6 pool carbon model and 4-5 data sets describing carbon pools and fluxes at each of the six sites (rows). Densities reflect 4 chains of 360k simulations each, with the first 20k simulations removed. SBL= Blue grama dominated site at the Sevilleta National Wildlife Refuge; SBK= Black grama dominated site at the Sevilleta National Wildlife Refuge; CPER=central plains experimental range; HPG=High Plains Grassland Research Station; HAR=Hays Agricultural Research Station; KNZ=Konza Prairie Biological Station. Transfer parameters (fx,y) dictate the proportion of C turnover in pool y transferring to pool x: f1=f43; f2=f53; f3=f54; f4=f64; f5=f45; f6=f65; f7=f46.

https://doi.org/10.5194/bg-2022-164
Preprint. Discussion started: 18 August 2022

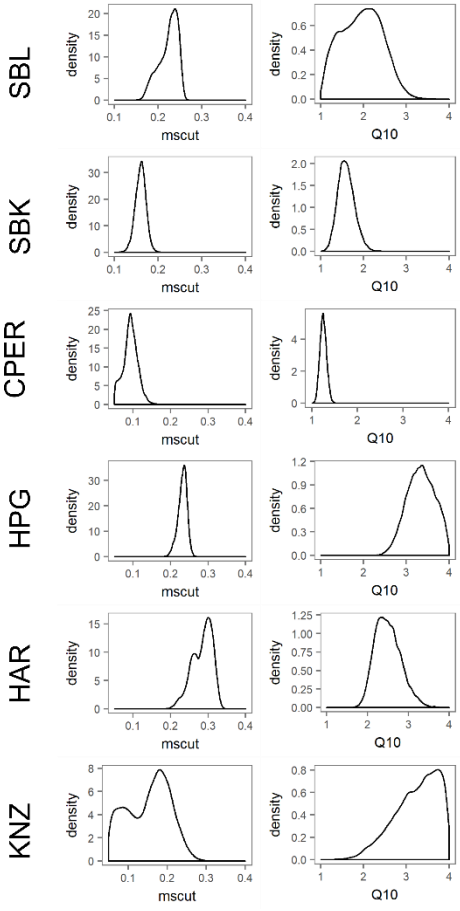

Figure A4. Density plots showing distribution of environmental scaling parameters (columns) dictating decomposition rates. We used data assimilation techniques with a 6 pool carbon model and 4-5 data sets describing carbon pools and fluxes at each of the six sites (rows). Densities reflect 4 chains of 360k simulations each, with the first 20k simulations removed. SBL= Blue grama dominated site at the Sevilleta National Wildlife Refuge; SBK= Black grama dominated site at the Sevilleta National Wildlife Refuge; CPER=central plains experimental range; HPG=High Plains Grassland Research Station; HAR=Hays Agricultural Research Station; KNZ=Konza Prairie Biological Station. mscut is the soil moisture level at which decomposition rates begin to become water limited; Q10 is the temperature sensitivity of decomposition.

https://doi.org/10.5194/bg-2022-164
Preprint. Discussion started: 18 August 2022

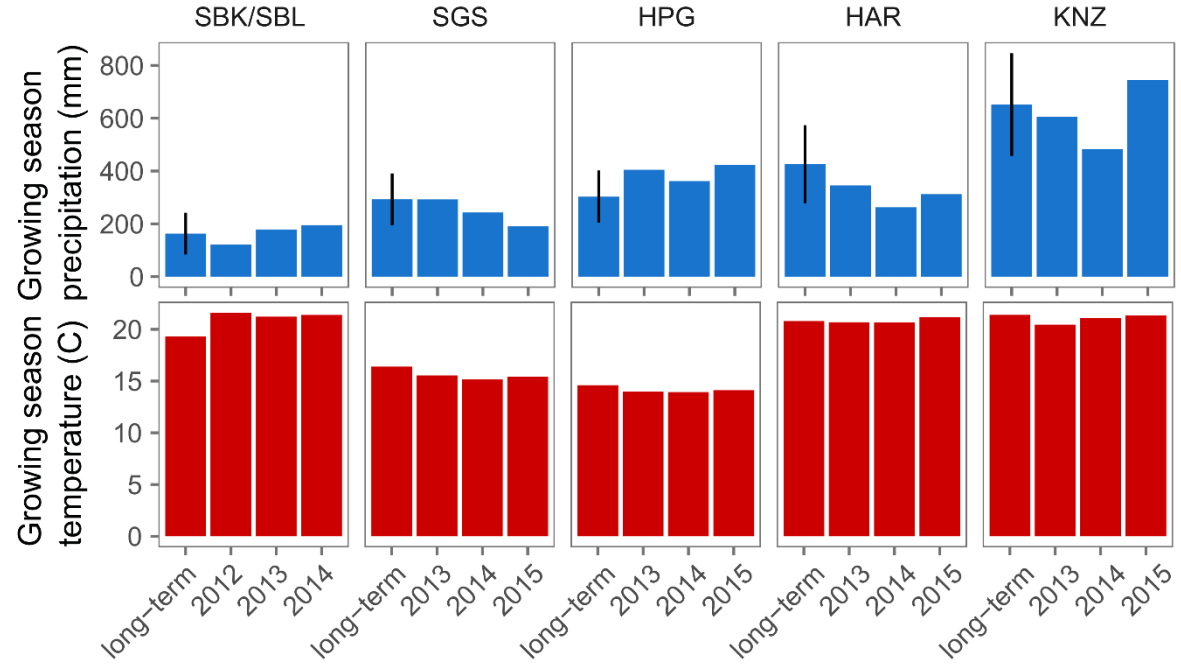

Figure A5. Precipitation and air temperature during the growing season (Apr-Oct for SBK and SBL, Apr-Sept for all other sites) during the three focal years at each site compared with the long-term mean precipitation and air temperature. Averages represent the period of 1982-2012 obtained from Knapp et al. 2015, and error bars represent 1 standard deviation from the mean.

https://doi.org/10.5194/bg-2022-164
Preprint. Discussion started: 18 August 2022

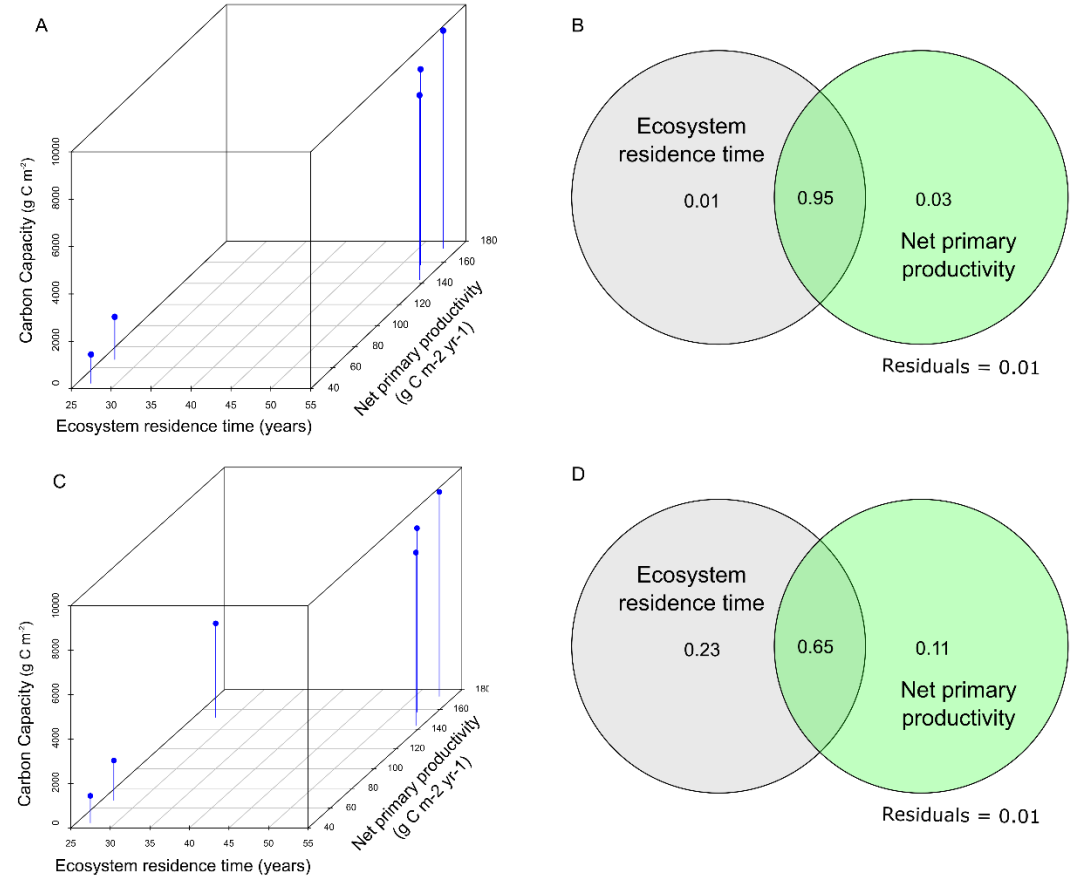

Figure A6. Three-dimensional plots (A,C) and variance partitioning results (B,D) showing the importance of ecosystem residence time and net primary productivity in making up the systems carbon capacity for our six focal ecosystems. A and B panels show results without KNZ, C and D include KNZ. In (B,D), numbers within the circles represent the amount of cross-site variance in carbon capacity explained solely by ecosystem residence time or net primary productivity. The number in the intersection represent variance explained jointly by both components.

https://doi.org/10.5194/bg-2022-164
Preprint. Discussion started: 18 August 2022

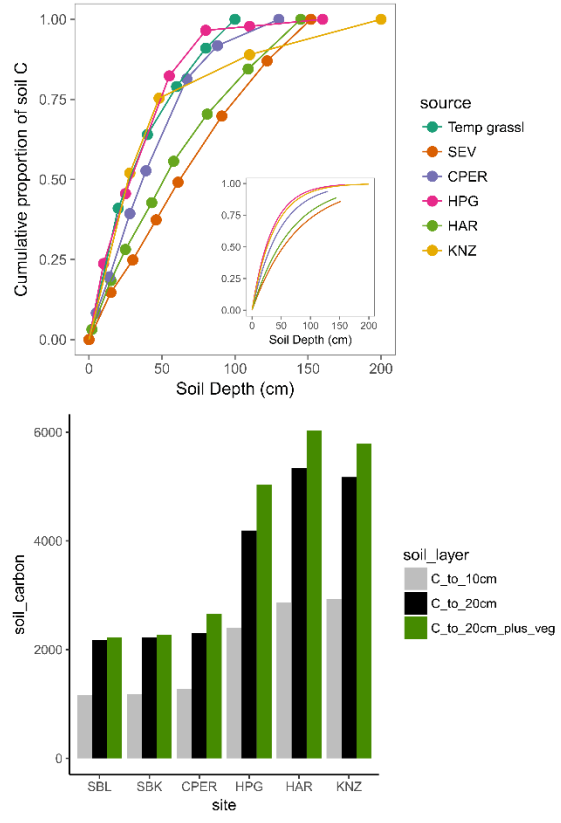

Figure A7. Top panel: Cumulative proportion of soil C along depth profile (main) and beta distribution of proportion by depth (inset). Data were obtained from the International Soil Carbon Network (see table B4) from areas close to study sites and having similar cover types and management regimes. In main panel, we included estimated proportions for temperate grasslands (Temp grass) from Jobbágy and Jackson (2000). Bottom panel: soil C measured at each study site from 0-10 cm and soil C estimates from 0-20 cm based on relationships in top panel. Estimates were obtained using: $C_{20}=C_{10}/C_{P10} \cdot C_{P20}$, where C_{10} is the soil C measured in the top 10 cm, C_{P10} is the proportion of C in the top 10 cm based on the beta regression, and C_{P20} is the proportion of C in the top 20 cm. Green bars represent soil C estimates from 0-20 cm plus vegetation C.

https://doi.org/10.5194/bg-2022-164
Preprint. Discussion started: 18 August 2022

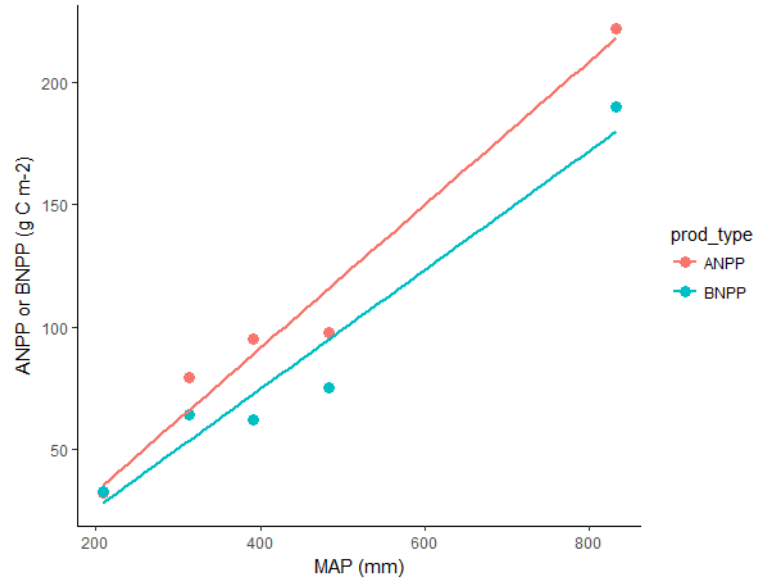

Figure A8. Average ANPP and BNPP simulation output across mean annual precipitation of our six grassland sites.

https://doi.org/10.5194/bg-2022-164
Preprint. Discussion started: 18 August 2022

Appendix B. Supplemental tables B1-B6

Table B1. Constraints and descriptions of carbon cycling and environmental scaling parameters used in data assimilation.

Param.	Default	Lower	Upper	Description	Units
c1	1.00E-03	1.00E-04	1.00E-02	The proportion of leaf C turning over each day	gC gC-1 day-1
c2	9.00E-03	1.00E-04	1.00E-02	The proportion of root C turning over each day	gC gC-1 day-1
c3	9.00E-03	5.00E-04	2.00E-02	The proportion of litter C turning over each day	gC gC-1 day-1
c4	1.50E-02	5.00E-03	5.00E-02	Proportion of fast SOM turning over each day	gC gC-1 day-1
c5	6.00E-04	1.00E-05	2.00E-03	Proportion of slow SOM turning over each day	gC gC-1 day-1
c6	2.00E-05	1.00E-08	3.00E-05	Proportion of passive SOM turning over each day	gC gC-1 day-1
f43	2.50E-01	3.00E-01	7.00E-01	Proportion of litter C turnover going to fast SOM pool	-
f53	1.00E-01	5.00E-02	1.50E-01	Proportion of litter C turnover going to slow SOM pool	-
f54	5.00E-01	2.50E-01	6.50E-01	Proportion of fast SOM turnover going to slow SOM pool	-
f64	4.00E-03	1.00E-03	8.00E-03	Proportion of litter C turnover going to passive SOM pool	-
f45	4.20E-01	1.00E-01	6.00E-01	Proportion of slow SOM turnover going to fast SOM pool	-
f65	5.00E-02	2.00E-03	7.00E-02	Proportion of slow C turnover going to passive SOM pool	-
f46	4.50E-01	3.00E-01	7.00E-01	Proportion of passive C turnover going to fast SOM pool	-
Q10	2.20E+00	1.00E+00	4.00E+00	Temperature sensitivity of decomposition	-
mscut	2.00E-01	1.00E-02	4.00E-01	Soil moisture level at which decomposition starts to become water limited	-

https://doi.org/10.5194/bg-2022-164
Preprint. Discussion started: 18 August 2022

Table B2. C cycling and environmental scaling parameters estimated via data assimilation with a six pool C model and 4-5 C pool and flux data sets for each of six grassland sites. 95% confidence intervals (CLl and CLu) are estimated from normal, log-normal, or Weibull distributions depending on the magnitude and direction of skew. Gelman-Rubin statistics (G-R) indicate convergence among independent chains.

	SBL				SBK			
Param	MLE	CLl	CLu	G-R	MLE	CLl	CLu	G-R
c1	0.009107	6.75E-03	1.00E-02	1.0	0.007977	0.004471	0.009999	1.0
c2	0.009405	7.70E-03	1.00E-02	1.0	0.00963	0.008492	0.01	1.0
c3	0.017967	1.24E-02	2.00E-02	1.0	0.00068	0.0005	0.001112	1.0
c4	0.017657	1.06E-02	2.67E-02	1.0	0.01101	0.006237	0.0172	1.0
c5	0.000232	1.00E-05	1.02E-03	1.0	0.000188	5.61E-05	0.000374	1.0
c6	1.46E-05	8.02E-07	2.87E-05	1.0	1.55E-05	1.41E-06	2.93E-05	1.0
f43	0.618122	3.74E-01	7.00E-01	1.0	0.593098	0.347119	0.699949	1.0
f53	0.110032	6.02E-02	1.50E-01	1.0	0.1055	0.056978	0.149515	1.0
f54	0.298433	2.50E-01	4.10E-01	1.0	0.312915	0.250004	0.435435	1.0
f64	0.004441	1.16E-03	7.71E-03	1.0	0.004506	0.001239	0.007792	1.0
f45	0.262651	1.00E-01	5.45E-01	1.0	0.31254	0.103977	0.552567	1.0
f65	0.036233	4.11E-03	6.77E-02	1.0	0.038417	0.005276	0.068779	1.0
f46	0.504545	3.17E-01	6.90E-01	1.0	0.497965	0.312594	0.681608	1.0
mscut	0.223073	1.78E-01	2.56E-01	1.0	0.159795	0.135553	0.18398	1.0
Q10	1.895981	1.07E+00	2.76E+00	1.0	1.597074	1.231482	1.986987	1.0

	CPER				HPG			
Param	MLE	CLl	CLu	G-R	MLE	CLl	CLu	G-R
c1	0.00746	0.005609	0.00966	1.0	0.007872	0.004192	0.009959	1.1
c2	0.001675	0.001518	0.00184	1.0	0.000488	0.000417	0.000562	1.0
c3	0.011091	0.006979	0.016717	1.0	0.018395	0.0143	0.019997	1.0
c4	0.017479	0.006234	0.041909	1.0	0.042184	0.024925	0.049978	1.1
c5	0.000128	0.0001	0.000181	1.0	0.000314	0.000164	0.000482	1.0
c6	1.49E-05	7.57E-07	2.86E-05	1.1	1.64E-05	1.97E-06	2.92E-05	1.2
f43	0.68024	0.618193	0.699996	1.0	0.576301	0.377749	0.699959	1.1
f53	0.137347	0.099531	0.149997	1.0	0.102849	0.057045	0.14747	1.3
f54	0.62252	0.546666	0.649987	1.0	0.574702	0.35944	0.649937	1.1
f64	0.004421	0.001187	0.007682	1.1	0.004583	0.001361	0.00768	1.2
f45	0.427899	0.176967	0.599756	1.0	0.388533	0.150328	0.587869	1.2
f65	0.040839	0.007248	0.069772	1.1	0.032149	0.002948	0.060738	1.1
f46	0.506596	0.316463	0.687456	1.0	0.473907	0.305835	0.667426	1.2
mscut	0.073406	0.014973	0.125796	1.0	0.231396	0.205847	0.253547	1.0
Q10	1.248167	1.10994	1.393126	1.0	3.482896	2.773369	3.950379	1.0

https://doi.org/10.5194/bg-2022-164
Preprint. Discussion started: 18 August 2022

	HAR				KNZ			
Param	MLE	CLl	CLu	G-R	MLE	CLl	CLu	G-R
c1	0.005025	0.002799	0.007883	1.0	0.001854	0.000722	0.00367	1.0
c2	0.000414	0.000257	0.0006	1.0	0.000967	0.000699	0.001413	1.0
c3	0.004664	0.002313	0.007928	1.0	0.013651	0.004197	0.019902	1.0
c4	0.026455	0.006518	0.047266	1.0	0.021989	0.005002	0.045437	1.0
c5	0.000171	0.0001	0.000308	1.0	0.000233	0.000106	0.00041	1.0
c6	1.41E-05	9.88E-07	2.88E-05	1.0	1.50E-05	1.46E-06	2.94E-05	1.0
f43	0.561531	0.34928	0.699978	1.0	0.531489	0.347243	0.696558	1.1
f53	0.102973	0.057002	0.146251	1.1	0.104992	0.05725	0.148682	1.1
f54	0.54796	0.303471	0.649941	1.3	0.586921	0.387489	0.649992	1.0
f64	0.004599	0.001247	0.007561	1.2	0.004439	0.001255	0.007846	1.0
f45	0.354072	0.125197	0.577835	1.3	0.39581	0.156163	0.599482	1.1
f65	0.03924	0.006196	0.069346	1.1	0.034188	0.004299	0.066817	1.1
f46	0.509573	0.327535	0.691565	1.0	0.490831	0.314648	0.683017	1.1
mscut	0.283857	0.231203	0.328458	1.0	0.114386	0.013291	0.232586	1.1
Q10	2.503186	1.929534	3.128982	1.0	3.445054	2.277028	3.999685	1.0

https://doi.org/10.5194/bg-2022-164
Preprint. Discussion started: 18 August 2022

Table B3. Cross correlations between Markov Chain Monte Carlo output of different model parameters during data assimilation.

site	param	c1	c2	c3	c4	c5	c6	f43	f53	f54	f64	f45	f65	f46	msc ut	Q10
SBL	c1	1	0.06	0.05	0.14	0.11	0.02	-0.04	-0.04	0.04	0.01	-0.02	0.02	-0.01	-0.09	-0.17
SBL	c2	0.06	1	0.04	0.13	0.02	0	-0.04	-0.02	0	0	0.01	0.01	0	0.05	-0.07
SBL	c3	0.05	0.04	1	0.1	-0.02	0.03	0.11	-0.01	-0.02	0.01	0.01	0.01	-0.02	0.01	-0.07
SBL	c4	0.14	0.13	0.1	1	0.47	0.02	0	-0.05	0.17	0.02	-0.05	0.02	-0.01	-0.18	-0.43
SBL	c5	0.11	0.02	-0.02	0.47	1	-0.03	-0.03	0.02	0.41	0.03	-0.21	0.06	0	-0.79	-0.86
SBL	c6	0.02	0	0.03	0.02	-0.03	1	0.01	-0.01	0	0.05	-0.02	-0.02	-0.05	0.02	0
SBL	f43	-0.04	-0.04	0.11	0	-0.03	0.01	1	0.01	-0.01	-0.02	0.04	0	-0.04	0.1	0.18
SBL	f53	-0.04	-0.02	-0.01	-0.05	0.02	-0.01	0.01	1	0.01	0	-0.04	0	0.01	0.04	0.09
SBL	f54	0.04	0	-0.02	0.17	0.41	0	-0.01	0.01	1	-0.03	-0.08	-0.01	0.03	-0.22	-0.21
SBL	f64	0.01	0	0.01	0.02	0.03	0.05	-0.02	0	-0.03	1	-0.04	-0.01	0	-0.04	-0.04
SBL	f45	-0.02	0.01	0.01	-0.05	-0.21	-0.02	0.04	-0.04	-0.08	-0.04	1	-0.03	0.03	0.25	0.28
SBL	f65	0.02	0.01	0.01	0.02	0.06	-0.02	0	0	-0.01	-0.01	-0.03	1	0.02	-0.03	-0.02
SBL	f46	-0.01	0	-0.02	-0.01	0	-0.05	-0.04	0.01	0.03	0	0.03	0.02	1	0.01	0.01
SBL	msc ut	-0.09	0.05	0.01	-0.18	-0.79	0.02	0.1	0.04	-0.22	-0.04	0.25	-0.03	0.01	1	0.87
SBL	Q10	-0.17	-0.07	-0.07	-0.43	-0.86	0	0.18	0.09	-0.21	-0.04	0.28	-0.02	0.01	0.87	1
SBK	c1	1.00	0.05	0.01	0.09	0.11	0.01	0.03	0.03	0.02	0.04	-0.01	-0.02	0.04	0.00	-0.16
SBK	c2	0.05	1.00	0.05	0.15	0.17	-0.01	-0.01	0.00	0.02	0.01	-0.01	0.00	0.01	0.07	-0.21
SBK	c3	0.01	0.05	1.00	0.05	-0.17	0.01	0.08	0.06	0.01	0.00	0.01	-0.02	0.00	0.05	-0.16
SBK	c4	0.09	0.15	0.05	1.00	0.52	-0.01	0.00	-0.02	0.06	-0.01	0.04	0.02	0.02	-0.01	-0.44
SBK	c5	0.11	0.17	-0.17	0.52	1.00	-0.07	0.09	0.01	0.27	0.01	0.11	0.06	0.01	-0.31	-0.75
SBK	c6	0.01	-0.01	0.01	-0.01	-0.07	1.00	0.04	0.04	-0.02	-0.06	-0.05	-0.01	0.03	-0.02	0.00
SBK	f43	0.03	-0.01	0.08	0.00	0.09	0.04	1.00	-0.05	0.09	0.00	0.01	-0.08	0.06	-0.02	0.00
SBK	f53	0.03	0.00	0.06	-0.02	0.01	0.04	-0.05	1.00	0.02	0.04	0.04	-0.08	-0.10	0.00	0.02
SBK	f54	0.02	0.02	0.01	0.06	0.27	-0.02	0.09	0.02	1.00	-0.02	0.02	-0.03	0.01	0.03	-0.02
SBK	f64	0.04	0.01	0.00	-0.01	0.01	-0.06	0.00	0.04	-0.02	1.00	-0.02	-0.01	0.00	-0.01	-0.01
SBK	f45	-0.01	-0.01	0.01	0.04	0.11	-0.05	0.01	0.04	0.02	-0.02	1.00	-0.06	0.00	0.06	0.07
SBK	f65	-0.02	0.00	-0.02	0.02	0.06	-0.01	-0.08	-0.08	-0.03	-0.01	-0.06	1.00	0.01	-0.01	-0.02
SBK	f46	0.04	0.01	0.00	0.02	0.01	0.03	0.06	-0.10	0.01	0.00	0.00	0.01	1.00	0.00	-0.01
SBK	msc ut	0.00	0.07	0.05	-0.01	-0.31	-0.02	-0.02	0.00	0.03	-0.01	0.06	-0.01	0.00	1.00	0.53
SBK	Q10	-0.16	-0.21	-0.16	-0.44	-0.75	0.00	0.00	0.02	-0.02	-0.01	0.07	-0.02	-0.01	0.53	1.00
CPER	c1	1.00	0.18	-0.05	-0.08	0.02	0.04	-0.01	0.04	0.05	0.01	0.02	0.02	-0.02	0.17	-0.16

https://doi.org/10.5194/bg-2022-164
Preprint. Discussion started: 18 August 2022

CPER	c2	0.18	1.00	0.09	0.00	0.06	0.02	-0.02	-0.03	-0.03	0.01	-0.02	-0.02	0.00	0.50	-0.47
CPER	c3	-0.05	0.09	1.00	-0.30	-0.01	0.07	0.08	0.02	-0.06	-0.07	-0.05	-0.04	0.00	0.08	-0.02
CPER	c4	-0.08	0.00	-0.30	1.00	0.01	-0.04	-0.03	-0.09	0.08	0.06	0.00	0.01	0.10	-0.03	0.01
CPER	c5	0.02	0.06	-0.01	0.01	1.00	-0.02	0.09	0.09	0.17	0.00	0.18	0.05	-0.03	0.03	-0.13
CPER	c6	0.04	0.02	0.07	-0.04	-0.02	1.00	0.03	0.05	0.05	0.02	-0.04	0.05	0.03	0.00	-0.02
CPER	f43	-0.01	-0.02	0.08	-0.03	0.09	0.03	1.00	-0.08	-0.11	0.03	-0.06	-0.02	-0.02	-0.02	0.08
CPER	f53	0.04	-0.03	0.02	-0.09	0.09	0.05	-0.08	1.00	-0.16	-0.13	-0.03	0.05	-0.04	-0.03	0.06
CPER	f54	0.05	-0.03	-0.06	0.08	0.17	0.05	-0.11	-0.16	1.00	0.01	-0.05	-0.05	0.01	-0.03	0.10
CPER	f64	0.01	0.01	-0.07	0.06	0.00	0.02	0.03	-0.13	0.01	1.00	-0.02	0.01	-0.03	0.01	0.00
CPER	f45	0.02	-0.02	-0.05	0.00	0.18	-0.04	-0.06	-0.03	-0.05	-0.02	1.00	0.01	-0.11	-0.01	0.07
CPER	f65	0.02	-0.02	-0.04	0.01	0.05	0.05	-0.02	0.05	-0.05	0.01	0.01	1.00	0.02	-0.03	0.01
CPER	f46	-0.02	0.00	0.00	0.10	-0.03	0.03	-0.02	-0.04	0.01	-0.03	-0.11	0.02	1.00	0.01	-0.01
CPER	msc ut	0.17	0.50	0.08	-0.03	0.03	0.00	-0.02	-0.03	-0.03	0.01	-0.01	-0.03	0.01	1.00	-0.03
CPER	Q10	-0.16	-0.47	-0.02	0.01	-0.13	-0.02	0.08	0.06	0.10	0.00	0.07	0.01	-0.01	-0.03	1.00
HPG	c1	1.00	-0.11	0.21	0.16	-0.10	-0.04	0.03	-0.07	-0.22	0.13	-0.17	-0.01	-0.08	-0.09	0.01
HPG	c2	-0.11	1.00	0.04	-0.04	0.46	-0.01	0.06	0.08	0.11	-0.06	0.02	-0.07	0.02	0.46	-0.44
HPG	c3	0.21	0.04	1.00	-0.07	-0.06	-0.02	-0.12	-0.13	-0.14	0.05	-0.01	0.00	-0.11	0.01	-0.03
HPG	c4	0.16	-0.04	-0.07	1.00	-0.07	-0.14	-0.13	0.02	-0.05	-0.01	-0.05	0.14	0.04	0.02	0.06
HPG	c5	-0.10	0.46	-0.06	-0.07	1.00	0.04	0.43	0.16	0.57	0.05	0.39	-0.10	0.12	0.02	-0.47
HPG	c6	-0.04	-0.01	-0.02	-0.14	0.04	1.00	0.21	0.05	0.14	0.12	0.03	-0.12	0.11	0.04	0.05
HPG	f43	0.03	0.06	-0.12	-0.13	0.43	0.21	1.00	0.05	0.17	-0.03	0.06	-0.17	0.11	0.04	-0.01
HPG	f53	-0.07	0.08	-0.13	0.02	0.16	0.05	0.05	1.00	0.01	-0.13	-0.13	-0.09	0.14	-0.02	-0.11
HPG	f54	-0.22	0.11	-0.14	-0.05	0.57	0.14	0.17	0.01	1.00	0.06	0.08	-0.17	0.11	0.11	-0.01
HPG	f64	0.13	-0.06	0.05	-0.01	0.05	0.12	-0.03	-0.13	0.06	1.00	0.15	0.02	0.00	-0.02	0.04
HPG	f45	-0.17	0.02	-0.01	-0.05	0.39	0.03	0.06	-0.13	0.08	0.15	1.00	-0.02	0.01	-0.04	-0.06
HPG	f65	-0.01	-0.07	0.00	0.14	-0.10	-0.12	-0.17	-0.09	-0.17	0.02	-0.02	1.00	-0.11	0.00	0.07
HPG	f46	-0.08	0.02	-0.11	0.04	0.12	0.11	0.11	0.14	0.11	0.00	0.01	-0.11	1.00	0.01	-0.01
HPG	msc ut	-0.09	0.46	0.01	0.02	0.02	0.04	0.04	-0.02	0.11	-0.02	-0.04	0.00	0.01	1.00	0.54
HPG	Q10	0.01	-0.44	-0.03	0.06	-0.47	0.05	-0.01	-0.11	-0.01	0.04	-0.06	0.07	-0.01	0.54	1.00
HAR	c1	1.00	0.86	0.55	0.04	0.45	0.10	-0.03	-0.10	-0.24	0.00	0.00	-0.06	0.00	0.66	-0.45
HAR	c2	0.86	1.00	0.63	0.03	0.51	0.08	-0.10	-0.10	-0.29	0.00	0.00	-0.07	0.03	0.76	-0.48
HAR	c3	0.55	0.63	1.00	0.02	0.32	0.01	-0.01	-0.06	-0.13	0.00	0.05	-0.08	0.03	0.48	-0.33
HAR	c4	0.04	0.03	0.02	1.00	-0.01	-0.06	-0.18	-0.02	0.15	0.05	-0.13	0.11	0.08	0.03	0.01
HAR	c5	0.45	0.51	0.32	-0.01	1.00	0.03	0.25	-0.10	0.23	0.04	0.23	-0.04	-0.03	0.31	-0.36
HAR	c6	0.10	0.08	0.01	-0.06	0.03	1.00	0.12	0.01	-0.06	-0.06	0.01	-0.05	-0.28	0.02	-0.13
HAR	f43	-0.03	-0.10	-0.01	-0.18	0.25	0.12	1.00	-0.30	-0.01	0.09	0.13	-0.10	-0.21	-0.12	0.03

https://doi.org/10.5194/bg-2022-164
Preprint. Discussion started: 18 August 2022

HAR	f53	-0.10	-0.10	-0.06	-0.02	-0.10	0.01	-0.30	1.00	-0.06	-0.12	-0.02	-0.01	-0.06	-0.03	0.12
HAR	f54	-0.24	-0.29	-0.13	0.15	0.23	-0.06	-0.01	-0.06	1.00	-0.05	-0.11	0.03	-0.01	-0.16	0.28
HAR	f64	0.00	0.00	0.00	0.05	0.04	-0.06	0.09	-0.12	-0.05	1.00	0.08	0.17	-0.04	-0.02	-0.02
HAR	f45	0.00	0.00	0.05	-0.13	0.23	0.01	0.13	-0.02	-0.11	0.08	1.00	-0.12	0.04	-0.01	0.00
HAR	f65	-0.06	-0.07	-0.08	0.11	-0.04	-0.05	-0.10	-0.01	0.03	0.17	-0.12	1.00	-0.10	-0.06	0.01
HAR	f46	0.00	0.03	0.03	0.08	-0.03	-0.28	-0.21	-0.06	-0.01	-0.04	0.04	-0.10	1.00	0.03	-0.02
HAR	msc ut	0.66	0.76	0.48	0.03	0.31	0.02	-0.12	-0.03	-0.16	-0.02	-0.01	-0.06	0.03	1.00	0.12
HAR	Q10	-0.45	-0.48	-0.33	0.01	-0.36	-0.13	0.03	0.12	0.28	-0.02	0.00	0.01	-0.02	0.12	1.00
KNZ	c1	1.00	0.52	0.04	-0.07	0.28	-0.07	-0.03	0.00	-0.07	-0.02	0.02	0.03	0.01	0.04	-0.48
KNZ	c2	0.52	1.00	0.01	-0.13	0.55	-0.05	-0.07	-0.02	-0.10	-0.06	0.03	0.04	0.02	0.08	-0.93
KNZ	c3	0.04	0.01	1.00	-0.05	0.08	0.09	0.10	0.04	0.02	-0.12	0.03	0.01	0.05	0.04	-0.01
KNZ	c4	-0.07	-0.13	-0.05	1.00	-0.21	-0.02	-0.05	0.11	0.03	0.08	-0.12	-0.04	-0.07	-0.09	0.11
KNZ	c5	0.28	0.55	0.08	-0.21	1.00	-0.05	0.19	0.08	0.23	-0.02	0.34	0.13	0.03	0.17	-0.48
KNZ	c6	-0.07	-0.05	0.09	-0.02	-0.05	1.00	0.02	0.06	0.12	-0.10	0.02	-0.08	-0.03	-0.02	0.03
KNZ	f43	-0.03	-0.07	0.10	-0.05	0.19	0.02	1.00	-0.02	0.05	0.10	0.01	0.01	-0.01	-0.04	0.07
KNZ	f53	0.00	-0.02	0.04	0.11	0.08	0.06	-0.02	1.00	0.05	0.09	0.05	-0.13	-0.12	0.04	0.04
KNZ	f54	-0.07	-0.10	0.02	0.03	0.23	0.12	0.05	0.05	1.00	0.00	-0.12	-0.02	-0.05	-0.02	0.09
KNZ	f64	-0.02	-0.06	-0.12	0.08	-0.02	-0.10	0.10	0.09	0.00	1.00	-0.14	0.07	-0.11	0.05	0.06
KNZ	f45	0.02	0.03	0.03	-0.12	0.34	0.02	0.01	0.05	-0.12	-0.14	1.00	0.08	0.14	0.09	-0.02
KNZ	f65	0.03	0.04	0.01	-0.04	0.13	-0.08	0.01	-0.13	-0.02	0.07	0.08	1.00	0.00	-0.07	-0.06
KNZ	f46	0.01	0.02	0.05	-0.07	0.03	-0.03	-0.01	-0.12	-0.05	-0.11	0.14	0.00	1.00	0.01	-0.02
KNZ	msc ut	0.04	0.08	0.04	-0.09	0.17	-0.02	-0.04	0.04	-0.02	0.05	0.09	-0.07	0.01	1.00	0.16
KNZ	Q10	-0.48	-0.93	-0.01	0.11	-0.48	0.03	0.07	0.04	0.09	0.06	-0.02	-0.06	-0.02	0.16	1.00

570

575

580

https://doi.org/10.5194/bg-2022-164
Preprint. Discussion started: 18 August 2022

Table B4. Descriptions of soil profile data sets obtained from the International Soil Carbon Network

Location	Site code	Latitude	Longitude	Profile depth (cm)
Sevilleta National Wildlife Refuge, New Mexico	81NM053005	34.18703	-107.21	152
Central Plains Experimental Range, Colorado	S1991CO123007	40.82806	-104.786	130
Cheyenne, Wyoming	S1989WY021007	41.20889	-104.931	160
Hays, Kansas	S1968KS051001	39.01528	-99.1258	145
Konza Priarie Biological Station, Kansas	KZP 1D	39.07597	-96.5638	200

585

590

595

600

https://doi.org/10.5194/bg-2022-164
Preprint. Discussion started: 18 August 2022

Biogeosciences Discussions Open Access EGU

Table B5. Variance partitioning results comparing among site variation in net primary productivity explained by site-level estimates of average annual precipitation, average annual temperature, soil bulk density, grass:forb, C3:C4, and annual species abundance.

	Variable 1	Variable2	Test	AdjR2	Fval	Pval
NPP	MAP	MAP	X1|X2	1.17	123.71	0.01
			X1X2 colin.	-0.21	NA	NA
			X2|X1	0.00	0.58	0.51
			X1+X2	0.96	63.84	<0.01
		Bulk Density	X1|X2	0.36	32.70	0.01
			X1X2 colin.	0.61	NA	NA
			X2|X1	-0.01	0.03	0.84
			X1+X2	0.95	53.74	0.02
		Grass:forb	X1|X2	0.09	11.44	0.05
			X1X2 colin.	0.87	NA	NA
			X2|X1	0.00	0.82	0.43
			X1+X2	0.96	68.27	<0.01
		C3:C4	X1|X2	1.15	103.19	<0.01
			X1X2 colin.	-0.18	NA	NA
			X2|X1	-0.01	0.04	0.83
			X1+X2	0.95	54.02	0.01
		Annual species abundance	X1|X2	0.50	74.70	0.01
			X1X2 colin.	0.47	NA	NA
			X2|X1	0.01	2.06	0.24
			X1+X2	0.97	90.77	<0.01
Eco_{RT}	MAT	MAP	X1|X2	0.73	6.57	0.11
			X1X2 colin.	-0.14	NA	NA
			X2|X1	-0.11	0.13	0.69
			X1+X2	0.52	3.29	0.14
		Bulk Density	X1|X2	0.35	3.60	0.18
			X1X2 colin.	0.24	NA	NA
			X2|X1	-0.13	0.02	0.90
			X1+X2	0.54	3.12	0.22
		Grass:forb	X1|X2	0.81	8.46	0.04
			X1X2 colin.	-0.22	NA	NA
			X2|X1	-0.03	0.75	0.31
			X1+X2	0.44	4.24	0.15
		C3:C4	X1|X2	0.55	5.34	0.14
			X1X2 colin.	0.04	NA	NA

https://doi.org/10.5194/bg-2022-164
Preprint. Discussion started: 18 August 2022

	X2|X1	-0.10	0.23	0.69
	X1+X2	0.51	3.44	0.12
Annual species abundance	X1|X2	0.58	5.31	0.13
	X1X2 colin.	0.01	NA	NA
	X2|X1	-0.13	0.03	0.94
	X1+X2	0.54	3.13	0.24

https://doi.org/10.5194/bg-2022-164
Preprint. Discussion started: 18 August 2022


Biogeosciences Discussions Open Access EGU

Table B6. Average soil moisture and soil temperature during June-September at our six focal grassland sites.

Site	Volumetric soil moisture (%)	Soil temperature (°C)
SBL	13.3	26.3
SBK	11.9	27.6
CPER	11.4	22.9
HPG	15.4	21.1
HAR	21.0	24.6
KNZ	20.9	24.0

630

635

640

645

https://doi.org/10.5194/bg-2022-164
Preprint. Discussion started: 18 August 2022

Appendix C. Detailed description of data collection and cleaning methods

C1 Aboveground net primary productivity (ANPP)

At CPER, HPG, HAR, and KNZ, ANPP was collected annually by clipping two 0.1 m^2 subplots per replicate in September, sorted to remove previous years' growth, dried at 60 C for 48 hours, and weighed. At SBK and SBL, ANPP was estimated using species-specific allometric methods (Muldavin et al. 2008) within four 1 m^2 subplots within each of the 10 control plots.

C2 Vegetative litter

Litter estimates were obtained by collecting previous year's biomass to ground level in the same subplots as ANPP. Litter was not present at SBL or SBK due to rapid decomposition at the soil surface at these sites, nor at KNZ due to annual burning.

C3 Belowground net primary productivity (BNPP) and root standing crop

BNPP was estimated from 0-20 cm at each site using two root ingrowth cores per plot (Persson 1980). Ingrowth cores were constructed from 2 mm fiberglass screen molded into a 5 cm diameter 22 cm long cylinder (2 cm was left above soil surface). In April-May, a soil auger was used to drill 20 cm deep in the soil. Ingrowth cores were then inserted, filled with sieved, root free soil from the site, and packed to approximate soil density. Ingrowth cores were removed in late September and stored at 4 C until processing. Samples were elutriated to separate root biomass from soil. Samples were sorted to remove soil organic matter, dried at 60 C for 48 hours, and weighed. Finally, samples were fired at 450 C and resulting ash subtracted from the biomass value to generate an ash free estimate of BNPP. 5 cm root standing crop samples were also taken from 0-20 cm in two subplots. Standing crop root samples were processed similarly to BNPP samples, with the exception that dead roots were sorted out of the samples at the same time as SOM.

C4 Soil CO_2 efflux

Surface soil respiration was calculated using measurements of soil CO_2 concentrations (GMP 220 series probes, Vaisala Corp., Helsinki, Finland) in three replicates per site at 5, 10, and 20 cm depths, combined with diffusion rates calculated using soil temperature and moisture data collected simultaneously with CO_2 concentration. See Vargas & Allen (2008), and Vargas et al. (2010) for more information about calculating soil respiration rates using this method. We averaged 15 minute soil respiration measurements between 10:00 am and 2:00 pm to obtain daily soil respiration values.

https://doi.org/10.5194/bg-2022-164
Preprint. Discussion started: 18 August 2022

C5 Soil moisture and temperature

Volumetric soil moisture integrated from 0-15 cm was measured in all 10 plots every 15 minutes using time domain reflectometry probes (CS-616 model, Campbell Scientific, Inc., Logan, UT, USA). Soil temperature was measured in 3 plots at 5 cm and 10 cm depths using thermocouples (K-type, OMEGA Engineering Inc., Stamford, CT, USA).

C6 Soil bulk density

Bulk density was measured at each site from ten 7 cm diameter soil cores taken 0-30 cm. Soil cores were extracted in segments to reduce compaction. All aboveground vegetation was removed, and cores were dried at 105 C for 48 hours, then weighed. Bulk density was then calculated as:

$$BD = \frac{M_{dry}}{\pi r^2 x\, D} \quad \text{(C1)}$$

Where M_{dry} is the dry mass, r is the radius, and D is the depth of the soil core.

C7 Meteorological data

Hourly air temperature, precipitation, relative humidity, vapor pressure deficit (VPD), and incident photosynthetically active radiation data were obtained from nearby weather stations to run the terrestrial ecosystem model (TECO; Weng and Luo, 2008). Gaps of < 10 time steps (hours) were filled by splining, and all splined sections examined to ensure values were within reasonable bounds. Gaps of longer time steps were filled from next closest meteorological stations of the same elevation. When unavailable, we calculated VPD as actual vapor pressure (e_a) minus saturation vapor pressure (e_s). e_a is estimated as:

$$e_a = \frac{RH}{100} e_s \quad \text{(C2)}$$

where RH is relative humidity, and e_s is estimated as:

$$e_s = 0.6108 e^{\frac{17.27t}{t+237.3}} \quad \text{(C3)}$$

where t is air temperature.

C8 Soil total organic carbon

At CPER, HGR, HAR, and KNZ, percent C was measured in three 2 cm diameter 10 cm deep soil cores per plot. Subsamples were aggregated, sieved with a 2 mm soil sieve to remove root material, dried, and ground. Samples were then

https://doi.org/10.5194/bg-2022-164
Preprint. Discussion started: 18 August 2022

measured for total C via dry combustion and grass chromatography using a LECO CN 2000 combustion analyzer (LECO Corp., Saint Joseph, MI, USA). For SBL and SBK, percent organic matter was estimated in soil from 0-10 cm depths from nearby areas having similar soils and vegetation to the EDGE sites. Organic matter values were then converted to percent C by dividing the percent organic matter by 1.72 (assumes 58% C stoichiometry of organic matter). Percent C for all sites was then converted to total C using:

$$C_T = D\ x\ BD\ x\ C_p x\ 10000 \quad \text{(C4)}$$

Where C_T is total carbon, D is the depth in cm to which the sample was collected, BD is the bulk density in g per cm^{-2}, and C_p is the proportion of carbon.

C9 Plant species abundance

Abundance of plant species was estimated visually in June and August in four 1 x 1 m^2 subplots per plot to the nearest percent. Species having less than 1% cover were rounded up to 1%. Calibrations of visual estimates were performed across researchers and with measurements seasonally. Maximum cover of each species was taken for each subplot, then all abundances were averaged across subplots to get plot-level estimates.

https://doi.org/10.5194/bg-2022-164
Preprint. Discussion started: 18 August 2022

Appendix D. Model evaluation text, Table D1, Figures D1-D3

Model validation exercises were conducted to compare the ability of the model to represent (1) average plant growth across sites and (2) variability of plant growth across years within each site. To this end, models were parameterized for each site based on soil texture, field capacity, wilting point, latitude, and root:shoot ratios. Additionally, maximum and minimum specific leaf area and Vcmax parameters were adjusted to better match measured above and belowground plant growth. Table 1 shows the parameter sets used for each site.

Empirical observations of ANPP and BNPP (n=10) were compared to leaf+stem biomass and root productivity from the model at the time of data collection. At CPER, HPG, HAR, and KNZ, ANPP was collected annually by clipping two 0.1 m2 subplots per replicate in September, sorted to remove previous years' growth (leaf litter), dried at 60 C for 48 hours, and weighed. At SBK and SBL, ANPP was estimated using species-specific allometric methods (Muldavin et al. 2008) within four 1m2 subplots within each of the 10 replicates. BNPP within each replicate at each site was estimated from 0-20 cm using two 20 cm x 5 cm diameter root ingrowth cores per plot (Persson 1980). See Appendix 3 for additional details about empirical data collection.

Models were spun up for 500 years using cycled meteorological data from each site – all carbon pools stabilized after 200-400 years. Then simulations were conducted for 2014-2017 for all sites. Empirical ANPP data were available from 2014-2017 for all sites, and BNPP was available for CPER, HPG, HAR, and KNZ for 2014-2017. BNPP was available at SBL and SBK from 2015-2017. To assess model performance, we calculated various validation metrics, including R2, RMSE, and the correlation coefficient.

Generally, cross-site averages of model output and observations were tightly correlated, but within-site model output was less correlated to interannual empirical observations (Table 1). However, it is important to note the variation associated with empirical measurements and that most model simulations fell within one standard error of empirical observations (error bars in Fig. D2 and D3). A notable exception to this occurred in 2014 at CPER and HPG sites, where BNPP was observed as much greater than model simulations. We are unsure what drove the high BNPP at these sites in 2014 since environmental conditions were within normal ranges (Fig. D1). It could be that other unmeasured variables (e.g., belowground animal activity, small mammal activity) were responsible for this high growth belowground.

Table D1. Model output for comparisons between empirical and simulated data.

Site	Productivity type	R2	RMSE	Correlation coefficient
means	anpp	0.988738	17.96882	0.994353
means	bnpp	0.93693	23.4836	0.967952
sbl	anpp	0.431519	9.568253	-0.6569
sbl	bnpp	0.009114	18.25828	-0.09547
sbk	anpp	0.667188	10.51358	0.816816
sbk	bnpp	0.059729	13.3254	-0.2444
cper	anpp	0.087017	33.30121	0.294986
cper	bnpp	0.181185	98.48398	0.425659
hpg	anpp	0.018955	35.10083	-0.13768
hpg	bnpp	0.022188	131.1703	0.148957

https://doi.org/10.5194/bg-2022-164
Preprint. Discussion started: 18 August 2022

har	anpp	0.526963	28.82132	0.725922
har	bnpp	0.330895	34.27893	0.575235
knz	anpp	0.004173	162.8426	-0.0646
knz	bnpp	0.637154	36.67331	-0.79822

anpp=aboveground net primary productivity, bnpp=belowground net primary productivity, sbl=Sevilleta National Wildlife Refuge blue grama grassland; sbk=Sevilleta National Wildlife Refuge black grama grassland; cper=Central Plains Experimental Range; hpg=High Plains Grasslands Research Station; har=Hays Agricultural Research Center; knz=Konza Prairie Biological Station

https://doi.org/10.5194/bg-2022-164
Preprint. Discussion started: 18 August 2022

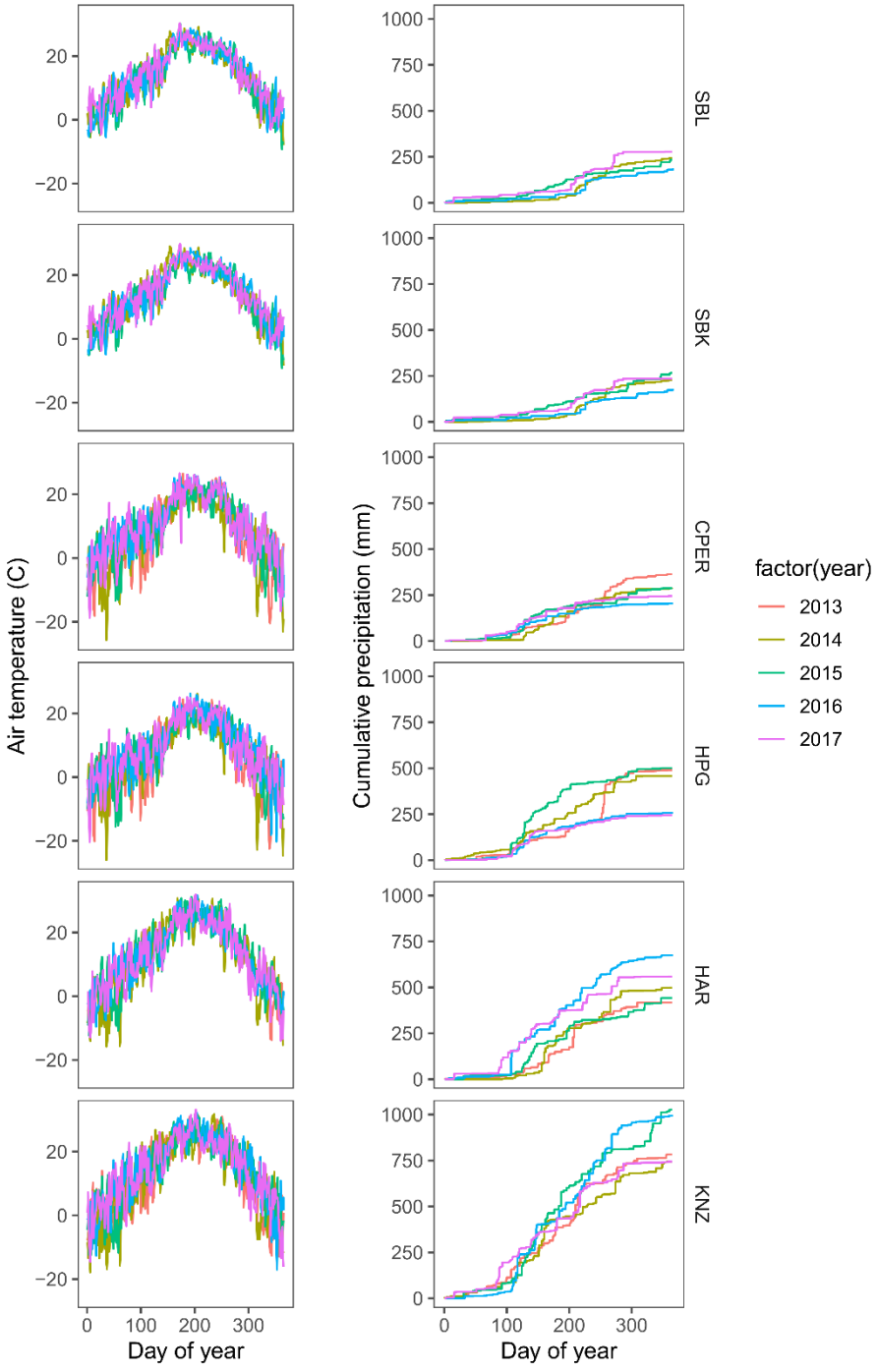

Figure D1. Cumulative hourly precipitation and hourly air temperature throughout each year simulated within each site.

https://doi.org/10.5194/bg-2022-164
Preprint. Discussion started: 18 August 2022

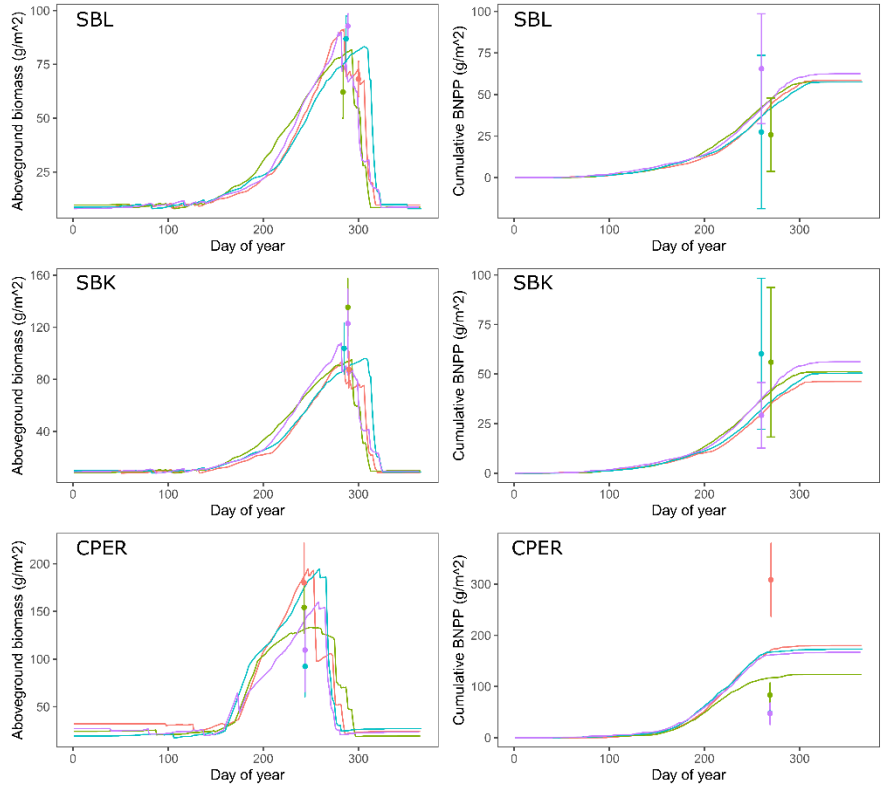

Figure D2. Within year patterns of simulated aboveground biomass and BNPP for SBL, SBK, and CPER, compared with empirical observations. Bars represent one standard deviation from the mean of the 10 replicate measurements. Years are represented as colors using the scale from Fig. 1.

https://doi.org/10.5194/bg-2022-164
Preprint. Discussion started: 18 August 2022

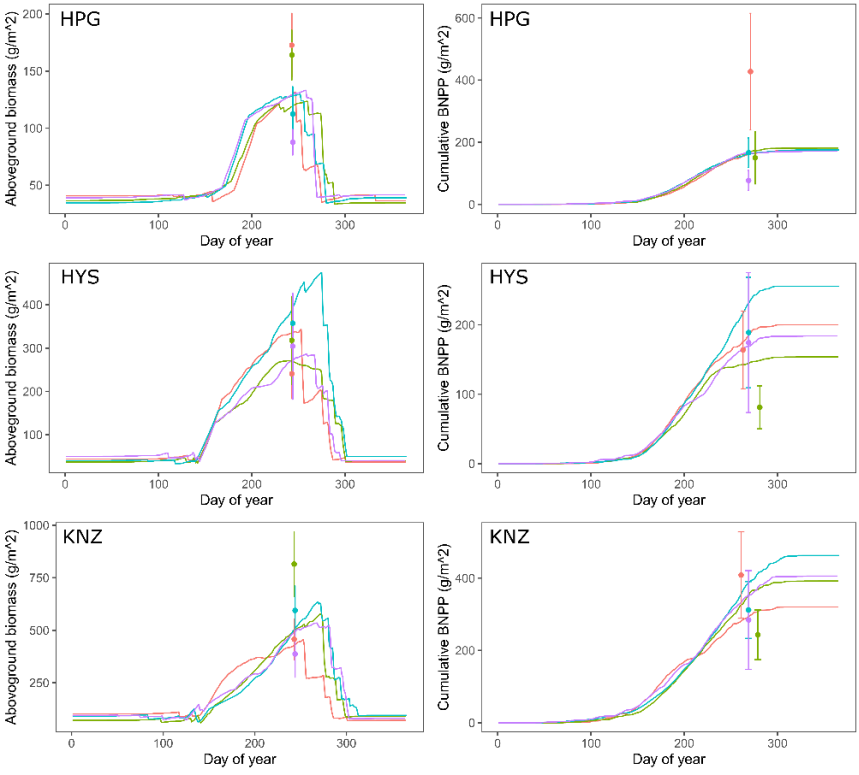

Figure D3. Within year patterns of simulated aboveground biomass and BNPP for HPG, HYS, and KNZ, compared with empirical observations. Bars represent one standard deviation from the mean of the 10 replicate measurements. Years are represented as colors using the scale from Fig. 1.

Code availability

R scripts to conduct data assimilation, calculate all metrics presented in the paper and statistical analyses publically available at https://github.com/wilcoxkr/AssessingCarbonCapacity. TECO model code is available on the ECOLAB website here: https://www2.nau.edu/luo-lab/?downloads.

Data availability

MCMC chains and raw empirical data is available upon request to the corresponding author.

https://doi.org/10.5194/bg-2022-164
Preprint. Discussion started: 18 August 2022

Author contributions

KRW, YL, MDS, SC, WP, and AKK designed the research project and participated in idea generation; KRW and ZS conducted analyses and model simulations; KRW led the writing process; all authors contributed to writing and editing process.

Competing interests

The authors declare that they have no conflict of interest

Acknowledgements

Support was provided to MDS and AKK by the Drought-Net Research Coordination Network funded by the US National Science Foundation (DEB-1354732), the Long Term Ecological Research Program of the US National Science Foundation (DEB-1655499), and by the Macrosystems Biology/Emerging Frontiers Programs (EF-1239559, EF-1137378). Support was provided to KRW by the Department of Energy (DE-SC0019037).

References

Austin, A. T. and Vivanco, L.: Plant litter decomposition in a semi-arid ecosystem controlled by photodegradation, Nature, 442, 555–558, https://doi.org/10.1038/nature05038, 2006.

Baisden, W. T., Parfitt, R. L., Ross, C., Schipper, L. A., and Canessa, S.: Evaluating 50 years of time-series soil radiocarbon data: towards routine calculation of robust C residence times, Biogeochemistry, 112, 129–137, https://doi.org/10.1007/s10533-011-9675-y, 2013.

Balesdent, J., Wagner, G. H., and Mariotti, A.: Soil organic matter turnover in long-term field experiments as revealed by carbon-13 natural abundance, Soil Science Society of America Journal, 52, 118–124, 1988.

Bell, C., McIntyre, N., Cox, S., Tissue, D., and Zak, J.: Soil Microbial Responses to Temporal Variations of Moisture and Temperature in a Chihuahuan Desert Grassland, Microb Ecol, 56, 153–167, https://doi.org/10.1007/s00248-007-9333-z, 2008.

Bhattacharyya, S. S., Ros, G. H., Furtak, K., Iqbal, H. M. N., and Parra-Saldívar, R.: Soil carbon sequestration – An interplay between soil microbial community and soil organic matter dynamics, Science of The Total Environment, 815, 152928, https://doi.org/10.1016/j.scitotenv.2022.152928, 2022.

Bird, M. I., Chivas, A. R., and Head, J.: A latitudinal gradient in carbon turnover times in forest soils, Nature, 381, 143–146, 1996.

Blume, E., Bischoff, M., Reichert, J. M., Moorman, T., Konopka, A., and Turco, R. F.: Surface and subsurface microbial biomass, community structure and metabolic activity as a function of soil depth and season, Applied Soil Ecology, 20, 171–181, https://doi.org/10.1016/S0929-1393(02)00025-2, 2002.

Brandt, L. A., King, J. Y., Hobbie, S. E., Milchunas, D. G., and Sinsabaugh, R. L.: The Role of Photodegradation in Surface Litter Decomposition Across a Grassland Ecosystem Precipitation Gradient, Ecosystems, 13, 765–781, https://doi.org/10.1007/s10021-010-9353-2, 2010.

Carvalhais, N., Forkel, M., Khomik, M., Bellarby, J., Jung, M., Migliavacca, M., Mu, M., Saatchi, S., Santoro, M., Thurner, M., Weber, U., Ahrens, B., Beer, C., Cescatti, A., Randerson, J. T., and Reichstein, M.: Global covariation of carbon turnover times with climate in terrestrial ecosystems, Nature, 514, 213–217, https://doi.org/10.1038/nature13731, 2014.

Chapin III, F. S., Matson, P. A., and Mooney, H. A.: Principles of Terrestrial Ecosystem Ecology, Springer-Verlag New York, Inc, New York, NY, 2011.

Chen, S., Huang, Y., Zou, J., and Shi, Y.: Mean residence time of global topsoil organic carbon depends on temperature, precipitation and soil nitrogen, Global and Planetary Change, 100, 99–108, https://doi.org/10.1016/j.gloplacha.2012.10.006, 2013.

Collins, S. L., Sinsabaugh, R. L., Crenshaw, C., Green, L., Porras-Alfaro, A., Stursova, M., and Zeglin, L. H.: Pulse dynamics and microbial processes in aridland ecosystems: Pulse dynamics in aridland soils, Journal of Ecology, 96, 413–420, https://doi.org/10.1111/j.1365-2745.2008.01362.x, 2008.

Daily, G. C., Polasky, S., Goldstein, J., Kareiva, P. M., Mooney, H. A., Pejchar, L., Ricketts, T. H., Salzman, J., and Shallenberger, R.: Ecosystem services in decision making: time to deliver, Frontiers in Ecology and the Environment, 7, 21–28, https://doi.org/10.1890/080025, 2009.

De Kauwe, M. G., Medlyn, B. E., Zaehle, S., Walker, A. P., Dietze, M. C., Wang, Y., Luo, Y., Jain, A. K., El-Masri, B., Hickler, T., Wårlind, D., Weng, E., Parton, W. J., Thornton, P. E., Wang, S., Prentice, I. C., Asao, S., Smith, B., McCarthy, H. R., Iversen, C. M., Hanson, P. J., Warren, J. M., Oren, R., and Norby, R. J.: Where does the carbon go? A model–data intercomparison of vegetation carbon allocation and turnover processes at two temperate forest free-air CO_2 enrichment sites, New Phytol, 203, 883–899, https://doi.org/10.1111/nph.12847, 2014.

Doetterl, S., Stevens, A., Six, J., Merckx, R., Van Oost, K., Casanova Pinto, M., Casanova-Katny, A., Muñoz, C., Boudin, M., Zagal Venegas, E., and Boeckx, P.: Soil carbon storage controlled by interactions between geochemistry and climate, Nature Geosci, 8, 780–783, https://doi.org/10.1038/ngeo2516, 2015.

Feng, J., Wang, J., Song, Y., and Zhu, B.: Patterns of soil respiration and its temperature sensitivity in grassland ecosystems across China, Biogeosciences, 15, 5329–5341, https://doi.org/10.5194/bg-15-5329-2018, 2018.

Fierer, N. and Schimel, J. P.: Effects of drying–rewetting frequency on soil carbon and nitrogen transformations, Soil Biology and Biochemistry, 34, 777–787, https://doi.org/10.1016/S0038-0717(02)00007-X, 2002.

Fierer, N., Schimel, J. P., and Holden, P. A.: Variations in microbial community composition through two soil depth profiles, Soil Biology and Biochemistry, 35, 167–176, https://doi.org/10.1016/S0038-0717(02)00251-1, 2003.

Freckleton, R. P.: The problems of prediction and scale in applied ecology: the example of fire as a management tool: Editorial, Journal of Applied Ecology, 41, 599–603, https://doi.org/10.1111/j.0021-8901.2004.00941.x, 2004.

Friend, A. D., Lucht, W., Rademacher, T. T., Keribin, R., Betts, R., Cadule, P., Ciais, P., Clark, D. B., Dankers, R., Falloon, P. D., Ito, A., Kahana, R., Kleidon, A., Lomas, M. R., Nishina, K., Ostberg, S., Pavlick, R., Peylin, P., Schaphoff, S., Vuichard, N., Warszawski, L., Wiltshire, A., and Woodward, F. I.: Carbon residence time dominates uncertainty in terrestrial vegetation responses to future climate and atmospheric CO_2, Proc. Natl. Acad. Sci. U.S.A., 111, 3280–3285, https://doi.org/10.1073/pnas.1222477110, 2014.

https://doi.org/10.5194/bg-2022-164
Preprint. Discussion started: 18 August 2022

García-Palacios, P., Shaw, E. A., Wall, D. H., and Hättenschwiler, S.: Temporal dynamics of biotic and abiotic drivers of litter decomposition, Ecol Lett, 19, 554–563, https://doi.org/10.1111/ele.12590, 2016.

Guzman, J. G. and Al-Kaisi, M. M.: Soil Carbon Dynamics and Carbon Budget of Newly Reconstructed Tall-grass Prairies in South Central Iowa, J. Environ. Qual., 39, 136–146, https://doi.org/10.2134/jeq2009.0063, 2010.

Hu, Z., Song, X., Wang, M., Ma, J., Zhang, Y., Xu, H.-J., Hu, Z., Zhu, X., Liu, H., Ma, J., Yu, Q., Ostle, N. J., Li, Y., and Yue, C.: Aridity influences root versus shoot contributions to steppe grassland soil carbon stock and its stability, Geoderma, 413, 115744, https://doi.org/10.1016/j.geoderma.2022.115744, 2022.

Hungate, B. A., Holland, E. A., Jackson, R. B., Chapin, F. S., Mooney, H. A., and Field, C. B.: The fate of carbon in grasslands under carbon dioxide enrichment, Nature, 388, 576–579, https://doi.org/10.1038/41550, 1997.

Huxman, T. E., Smith, M. D., Fay, P. A., Knapp, A. K., Shaw, M. R., Loik, M. E., Smith, S. D., Tissue, D. T., Zak, J. C., Weltzin, J. F., Pockman, W. T., Sala, O. E., Haddad, B. M., Harte, J., Koch, G. W., Schwinning, S., Small, E. E., and Williams, D. G.: Convergence across biomes to a common rain-use efficiency, Nature, 429, 651–654, https://doi.org/10.1038/nature02561, 2004.

IPCC, 2022: Summary for Policymakers [H.-O. Pörtner, D.C. Roberts, E.S. Poloczanska, K. Mintenbeck, M. Tignor, A. Alegría, M. Craig, S. Langsdorf, S. Löschke, V. Möller, A. Okem (eds.)]. In: Climate Change 2022: Impacts, Adaptation and Vulnerability. Contribution of Working Group II to the Sixth Assessment Report of the Intergovernmental Panel on Climate Change [H.-O. Pörtner, D.C. Roberts, M. Tignor, E.S. Poloczanska, K. Mintenbeck, A. Alegría, M. Craig, S. Langsdorf, S. Löschke, V. Möller, A. Okem, B. Rama (eds.)]. Cambridge University Press, Cambridge, UK and New York, NY, USA, pp. 3–33, doi:10.1017/9781009325844.001.

Jackson, R. B., Canadell, J., Ehleringer, J. R., Mooney, H. A., Sala, O. E., and Schulze, E. D.: A global analysis of root distributions for terrestrial biomes, Oecologia, 108, 389–411, https://doi.org/10.1007/BF00333714, 1996.

Jobbágy, E. G. and Jackson, R. B.: THE VERTICAL DISTRIBUTION OF SOIL ORGANIC CARBON AND ITS RELATION TO CLIMATE AND VEGETATION, Ecological Applications, 10, 14, 2000.

Johnson, L. C. and Matchett, J. R.: FIRE AND GRAZING REGULATE BELOWGROUND PROCESSES IN TALLGRASS PRAIRIE, Ecology, 82, 3377–3389, https://doi.org/10.1890/0012-9658(2001)082[3377:FAGRBP]2.0.CO;2, 2001.

Knapp, A. K., Briggs, J. M., Hartnett, D. C., and Collins, S. L.: Grassland dynamics: Long-term ecological research in tallgrass prairie, Oxford University Press, Inc., New York, NY, 1998.

Knapp, A. K., Carroll, C. J. W., Denton, E. M., La Pierre, K. J., Collins, S. L., and Smith, M. D.: Differential sensitivity to regional-scale drought in six central US grasslands, Oecologia, 177, 949–957, https://doi.org/10.1007/s00442-015-3233-6, 2015.

Lal, R.: Soil Carbon Sequestration Impacts on Global Climate Change and Food Security, Science, 304, 1623–1627, https://doi.org/10.1126/science.1097396, 2004.

Leppälammi-Kujansuu, J., Aro, L., Salemaa, M., Hansson, K., Kleja, D. B., and Helmisaari, H.-S.: Fine root longevity and carbon input into soil from below- and aboveground litter in climatically contrasting forests, Forest Ecology and Management, 326, 79–90, https://doi.org/10.1016/j.foreco.2014.03.039, 2014.

Luo, Y., Keenan, T. F., and Smith, M.: Predictability of the terrestrial carbon cycle, Glob Change Biol, 21, 1737–1751, https://doi.org/10.1111/gcb.12766, 2015.

Luo, Y., Shi, Z., Lu, X., Xia, J., Liang, J., Jiang, J., Wang, Y., Smith, M. J., Jiang, L., Ahlström, A., Chen, B., Hararuk, O., Hastings, A., Hoffman, F., Medlyn, B., Niu, S., Rasmussen, M., Todd-Brown, K., and Wang, Y.-P.: Transient dynamics of terrestrial carbon storage: mathematical foundation and its applications, Biogeosciences, 14, 145–161, https://doi.org/10.5194/bg-14-145-2017, 2017.

Mathieu, J. A., Hatté, C., Balesdent, J., and Parent, É.: Deep soil carbon dynamics are driven more by soil type than by climate: a worldwide meta-analysis of radiocarbon profiles, Glob Change Biol, 21, 4278–4292, https://doi.org/10.1111/gcb.13012, 2015.

Maurer, G. E., Hallmark, A. J., Brown, R. F., Sala, O. E., and Collins, S. L.: Sensitivity of primary production to precipitation across the United States, Ecol Lett, 23, 527–536, https://doi.org/10.1111/ele.13455, 2020.

Mokany, K., Raison, R. J., and Prokushkin, A. S.: Critical analysis of root : shoot ratios in terrestrial biomes: ROOT : SHOOT RATIOS IN TERRESTRIAL BIOMES, Global Change Biology, 12, 84–96, https://doi.org/10.1111/j.1365-2486.2005.001043.x, 2006.

Moore, S., Adu-Bredu, S., Duah-Gyamfi, A., Addo-Danso, S. D., Ibrahim, F., Mbou, A. T., Grandcourt, A., Valentini, R., Nicolini, G., Djagbletey, G., Owusu-Afriyie, K., Gvozdevaite, A., Oliveras, I., Ruiz-Jaen, M. C., and Malhi, Y.: Forest biomass, productivity and carbon cycling along a rainfall gradient in West Africa, Glob Change Biol, 24, e496–e510, https://doi.org/10.1111/gcb.13907, 2018.

Luke Nave, Kris Johnson, Catharine van Ingen, Deborah Agarwal, Marty Humphrey, and Norm Beekwilder, International Soil Carbon Network (ISCN) Database V3-1, 10.17040/ISCN/1305039. Accessed July 2017.

Naylor, D., Sadler, N., Bhattacharjee, A., Graham, E. B., Anderton, C. R., McClure, R., Lipton, M., Hofmockel, K. S., and Jansson, J. K.: Soil Microbiomes Under Climate Change and Implications for Carbon Cycling, Annu. Rev. Environ. Resour., 45, 29–59, https://doi.org/10.1146/annurev-environ-012320-082720, 2020.

Jari Oksanen, Gavin L. Simpson, F. Guillaume Blanchet, Roeland Kindt, Pierre Legendre, Peter R. Minchin, R.B. O'Hara, Peter Solymos, M. Henry H. Stevens, Eduard Szoecs, Helene Wagner, Matt Barbour, Michael Bedward, Ben Bolker, Daniel Borcard, Gustavo Carvalho, Michael Chirico, Miquel De Caceres, Sebastien Durand, Heloisa Beatriz Antoniazi Evangelista, Rich FitzJohn, Michael Friendly, Brendan Furneaux, Geoffrey Hannigan, Mark O. Hill, Leo Lahti, Dan McGlinn, Marie-Helene Ouellette, Eduardo Ribeiro Cunha, Tyler Smith, Adrian Stier, Cajo J.F. Ter Braak and James Weedon (2022). vegan: Community Ecology Package. R package version 2.6-2. https://CRAN.R-project.org/package=vegan

Pan, Y., Birdsey, R. A., Fang, J., Houghton, R., Kauppi, P. E., Kurz, W. A., Phillips, O. L., Shvidenko, A., Lewis, S. L., Canadell, J. G., Ciais, P., Jackson, R. B., Pacala, S. W., McGuire, A. D., Piao, S., Rautiainen, A., Sitch, S., and Hayes, D.: A Large and Persistent Carbon Sink in the World's Forests, Science, 333, 988–993, https://doi.org/10.1126/science.1201609, 2011.

Parton, W., Silver, W. L., Burke, I. C., Grassens, L., Harmon, M. E., Currie, W. S., King, J. Y., Adair, E. C., Brandt, L. A., Hart, S. C., and Fasth, B.: Global-Scale Similarities in Nitrogen Release Patterns During Long-Term Decomposition, Science, 315, 361–364, https://doi.org/10.1126/science.1134853, 2007.

Petrie, M. D., Collins, S. L., Swann, A. M., Ford, P. L., and Litvak, M. E.: Grassland to shrubland state transitions enhance carbon sequestration in the northern Chihuahuan Desert, Global Change Biology, 21, 1226–1235, https://doi.org/10.1111/gcb.12743, 2015.

Poulter, B., Frank, D., Ciais, P., Myneni, R. B., Andela, N., Bi, J., Broquet, G., Canadell, J. G., Chevallier, F., Liu, Y. Y., Running, S. W., Sitch, S., and van der Werf, G. R.: Contribution of semi-arid ecosystems to interannual variability of the global carbon cycle, Nature, 509, 600–603, https://doi.org/10.1038/nature13376, 2014.

R Core Team (2022). R: A language and environment for statistical computing. R Foundation for Statistical Computing, Vienna, Austria. https://www.R-project.org/

Rees, R. M., Bingham, I. J., Baddeley, J. A., and Watson, C. A.: The role of plants and land management in sequestering soil carbon in temperate arable and grassland ecosystems, Geoderma, 128, 130–154, https://doi.org/10.1016/j.geoderma.2004.12.020, 2005.

Saiz, G., Bird, M. I., Domingues, T., Schrodt, F., Schwarz, M., Feldpausch, T. R., Veenendaal, E., Djagbletey, G., Hien, F., Compaore, H., Diallo, A., and Lloyd, J.: Variation in soil carbon stocks and their determinants across a precipitation gradient in West Africa, Glob Change Biol, 18, 1670–1683, https://doi.org/10.1111/j.1365-2486.2012.02657.x, 2012.

Sala, O. E., Parton, W. J., Joyce, L. A., and Lauenroth, W. K.: Primary Production of the Central Grassland Region of the United States, Ecology, 69, 40–45, https://doi.org/10.2307/1943158, 1988.

Sala, O. E., Gherardi, L. A., Reichmann, L., Jobbágy, E., and Peters, D.: Legacies of precipitation fluctuations on primary production: theory and data synthesis, Phil. Trans. R. Soc. B, 367, 3135–3144, https://doi.org/10.1098/rstb.2011.0347, 2012.

Schenk, H. J. and Jackson, R. B.: THE GLOBAL BIOGEOGRAPHY OF ROOTS, Ecological Monographs, 72, 311–328, https://doi.org/10.1890/0012-9615(2002)072[0311:TGBOR]2.0.CO;2, 2002.

Seastedt, T. R.: Mass, Nitrogen, and Phosphorus Dynamics in Foliage and Root Detritus of Tallgrass Prairie, Ecology, 69, 59–65, https://doi.org/10.2307/1943160, 1988.

Shi, Z., Thomey, M. L., Mowll, W., Litvak, M., Brunsell, N. A., Collins, S. L., Pockman, W. T., Smith, M. D., Knapp, A. K., and Luo, Y.: Differential effects of extreme drought on production and respiration: synthesis and modeling analysis, Biogeosciences, 11, 621–633, https://doi.org/10.5194/bg-11-621-2014, 2014.

Shi, Z., Xu, X., Hararuk, O., Jiang, L., Xia, J., Liang, J., Li, D., and Luo, Y.: Experimental warming altered rates of carbon processes, allocation, and carbon storage in a tallgrass prairie, Ecosphere, 6, art210, https://doi.org/10.1890/ES14-00335.1, 2015.

Sinsabaugh, R. L., Lauber, C. L., Weintraub, M. N., Ahmed, B., Allison, S. D., Crenshaw, C., Contosta, A. R., Cusack, D., Frey, S., Gallo, M. E., Gartner, T. B., Hobbie, S. E., Holland, K., Keeler, B. L., Powers, J. S., Stursova, M., Takacs-Vesbach, C., Waldrop, M. P., Wallenstein, M. D., Zak, D. R., and Zeglin, L. H.: Stoichiometry of soil enzyme activity at global scale: Stoichiometry of soil enzyme activity, Ecology Letters, 11, 1252–1264, https://doi.org/10.1111/j.1461-0248.2008.01245.x, 2008.

Smith, P.: Do grasslands act as a perpetual sink for carbon?, Glob Change Biol, 20, 2708–2711, https://doi.org/10.1111/gcb.12561, 2014.

Soong, J. L. and Cotrufo, M. F.: Annual burning of a tallgrass prairie inhibits C and N cycling in soil, increasing recalcitrant pyrogenic organic matter storage while reducing N availability, Glob Change Biol, 21, 2321–2333, https://doi.org/10.1111/gcb.12832, 2015.

Soussana, J. F., Allard, V., Pilegaard, K., Ambus, P., Amman, C., Campbell, C., Ceschia, E., Clifton-Brown, J., Czobel, S., Domingues, R., Flechard, C., Fuhrer, J., Hensen, A., Horvath, L., Jones, M., Kasper, G., Martin, C., Nagy, Z., Neftel, A., Raschi, A., Baronti, S., Rees, R. M., Skiba, U., Stefani, P., Manca, G., Sutton, M., Tuba, Z., and Valentini, R.: Full accounting of the greenhouse gas (CO2, N2O, CH4) budget of nine European grassland sites, Agriculture, Ecosystems & Environment, 121, 121–134, https://doi.org/10.1016/j.agee.2006.12.022, 2007.

Stielstra, C. M., Lohse, K. A., Chorover, J., McIntosh, J. C., Barron-Gafford, G. A., Perdrial, J. N., Litvak, M., Barnard, H. R., and Brooks, P. D.: Climatic and landscape influences on soil moisture are primary determinants of soil carbon fluxes in seasonally snow-covered forest ecosystems, Biogeochemistry, 123, 447–465, https://doi.org/10.1007/s10533-015-0078-3, 2015.

Sulman, B. N., Moore, J. A. M., Abramoff, R., Averill, C., Kivlin, S., Georgiou, K., Sridhar, B., Hartman, M. D., Wang, G., Wieder, W. R., Bradford, M. A., Luo, Y., Mayes, M. A., Morrison, E., Riley, W. J., Salazar, A., Schimel, J. P., Tang, J., and Classen, A. T.: Multiple models and experiments underscore large uncertainty in soil carbon dynamics, Biogeochemistry, 141, 109–123, https://doi.org/10.1007/s10533-018-0509-z, 2018.

Sulzman, E. W., Brant, J. B., Bowden, R. D., and Lajtha, K.: Contribution of aboveground litter, belowground litter, and rhizosphere respiration to total soil CO2 efflux in an old growth coniferous forest, Biogeochemistry, 73, 231–256, https://doi.org/10.1007/s10533-004-7314-6, 2005.

Taylor, J. P., Wilson, B., Mills, M. S., and Burns, R. G.: Comparison of microbial numbers and enzymatic activities in surface soils and subsoils using various techniques, Soil Biology and Biochemistry, 34, 387–401, https://doi.org/10.1016/S0038-0717(01)00199-7, 2002.

Telles, E. de C. C., de Camargo, P. B., Martinelli, L. A., Trumbore, S. E., da Costa, E. S., Santos, J., Higuchi, N., and Oliveira, R. C.: Influence of soil texture on carbon dynamics and storage potential in tropical forest soils of Amazonia: CARBON STORAGE POTENTIAL OF TROPICAL SOILS, Global Biogeochem. Cycles, 17, n/a-n/a, https://doi.org/10.1029/2002GB001953, 2003.

Thomey, M. L., Collins, S. L., Vargas, R., Johnson, J. E., Brown, R. F., Natvig, D. O., and Friggens, M. T.: Effect of precipitation variability on net primary production and soil respiration in a Chihuahuan Desert grassland: PRECIPITATION VARIABILITY IN DESERT GRASSLAND, Global Change Biology, 17, 1505–1515, https://doi.org/10.1111/j.1365-2486.2010.02363.x, 2011.

Todd-Brown, K. E. O., Randerson, J. T., Hopkins, F., Arora, V., Hajima, T., Jones, C., Shevliakova, E., Tjiputra, J., Volodin, E., Wu, T., Zhang, Q., and Allison, S. D.: Changes in soil organic carbon storage predicted by Earth system models during the 21st century, Biogeosciences, 11, 2341–2356, https://doi.org/10.5194/bg-11-2341-2014, 2014.

Wang, Y., Xie, Z., and Jia, B.: Incorporation of a dynamic root distribution into CLM4.5: Evaluation of carbon and water fluxes over the Amazon, Adv. Atmos. Sci., 33, 1047–1060, https://doi.org/10.1007/s00376-016-5226-8, 2016.

Weng, E. and Luo, Y.: Soil hydrological properties regulate grassland ecosystem responses to multifactor global change: A modeling analysis, J. Geophys. Res., 113, G03003, https://doi.org/10.1029/2007JG000539, 2008.

Wiesmeier, M., Urbanski, L., Hobley, E., Lang, B., von Lützow, M., Marin-Spiotta, E., van Wesemael, B., Rabot, E., Ließ, M., Garcia-Franco, N., Wollschläger, U., Vogel, H.-J., and Kögel-Knabner, I.: Soil organic carbon storage as a key function of soils - A review of drivers and indicators at various scales, Geoderma, 333, 149–162, https://doi.org/10.1016/j.geoderma.2018.07.026, 2019.

Wilcox, K. R., Blair, J. M., and Knapp, A. K.: Stability of grassland soil C and N pools despite 25 years of an extreme climatic and disturbance regime: PRECIPITATION IMPACTS ON SOIL C AND N, J. Geophys. Res. Biogeosci., 121, 1934–1945, https://doi.org/10.1002/2016JG003370, 2016.

Williams, M. A. and Rice, C. W.: Seven years of enhanced water availability influences the physiological, structural, and functional attributes of a soil microbial community, Applied Soil Ecology, 35, 535–545, https://doi.org/10.1016/j.apsoil.2006.09.014, 2007.

Wu, D., Piao, S., Zhu, D., Wang, X., Ciais, P., Bastos, A., Xu, X., and Xu, W.: Accelerated terrestrial ecosystem carbon turnover and its drivers, Glob Change Biol, 26, 5052–5062, https://doi.org/10.1111/gcb.15224, 2020.

Wu, Z., Dijkstra, P., Koch, G. W., Peñuelas, J., and Hungate, B. A.: Responses of terrestrial ecosystems to temperature and precipitation change: a meta-analysis of experimental manipulation: META-ANALYSIS OF EXPERIMENTAL MANIPULATION, Global Change Biology, 17, 927–942, https://doi.org/10.1111/j.1365-2486.2010.02302.x, 2011.

Xu, T., White, L., Hui, D., and Luo, Y.: Probabilistic inversion of a terrestrial ecosystem model: Analysis of uncertainty in parameter estimation and model prediction: PROBABILISTIC INVERSION OF TERRESTRIAL ECOSYSTEM, Global Biogeochem. Cycles, 20, n/a-n/a, https://doi.org/10.1029/2005GB002468, 2006.

You, Y., Wang, J., Huang, X., Tang, Z., Liu, S., and Sun, O. J.: Relating microbial community structure to functioning in forest soil organic carbon transformation and turnover, Ecol Evol, 4, 633–647, https://doi.org/10.1002/ece3.969, 2014.

Zhao, Y. F., Wang, X., Jiang, S. L., Zhou, X. H., Liu, H. Y., Xiao, J. J., Hao, Z. G., and Wang, K. C.: Climate and geochemistry interactions at different altitudes influence soil organic carbon turnover times in alpine grasslands, Agriculture, Ecosystems & Environment, 320, 107591, https://doi.org/10.1016/j.agee.2021.107591, 2021.

Zhou, T. and Luo, Y.: Spatial patterns of ecosystem carbon residence time and NPP-driven carbon uptake in the conterminous United States: CARBON RESIDENCE TIME AND CARBON UPTAKE, Global Biogeochem. Cycles, 22, n/a-n/a, https://doi.org/10.1029/2007GB002939, 2008.

Zhou, X., Zhou, T., and Luo, Y.: Uncertainties in carbon residence time and NPP-driven carbon uptake in terrestrial ecosystems of the conterminous USA: a Bayesian approach, Tellus B: Chemical and Physical Meteorology, 64, 17223, https://doi.org/10.3402/tellusb.v64i0.17223, 2012.